

Article

Geochronology, Geochemical Characterization and Tectonic Background of Volcanic Rocks of the Longjiang Formation in the Lengjimanda Plate Area, Middle Da Hinggan Mountains

Shi-Chang Wang¹, Yu-Jie Hao^{1,2,*}, Lu Shi^{3,*}, Zhen Tang³ and Shuang Zhu⁴¹ College of Earth Sciences, Jilin University, Changchun 130061, China; wsc1873818566@126.com² Key Laboratory of Mineral Resources Evaluation of Northeast Asia, Ministry of Natural Resources, Changchun 130061, China³ Shenyang Center, China Geological Survey, Shenyang 110034, China; tangzhen@mail.cgs.gov.cn⁴ The First Geological Survey of Jilin Province, Changchun 130061, China; zhushuang0523@163.com

* Correspondence: haoyujie@jlu.edu.cn (Y.-J.H.); shilu@mail.cgs.gov.cn (L.S.)

Abstract: The Lengjimanda plate is situated in the middle section of the Da Hinggan mountains, in the eastern section of the Tianshan Xingmeng orogenic belt. To determine the formation age of the volcanic rocks in the Longjiang formation in this area, to explore their origin and tectonic background, and to reconstruct the geodynamic evolution of the region, this study conducted petrological, zircon U–Pb geochronological, geochemical, and isotopic analyses of the volcanic rocks in the Longjiang formation. The Longjiang formation's volcanic rocks are primarily composed of trachyandesite, trachyte trachydacite, and andesite, which are intermediate basic volcanic rocks. They are enriched in large-ion lithophile elements, are depleted in high-field-strength elements, are significantly fractionated between light and heavy rare earth elements, and exhibit a moderate negative Eu anomaly in most samples. The results of the LA–ICP–MS zircon U–Pb dating indicate that the volcanic rocks in this group were formed in the Early Cretaceous period at 129.1 ± 0.82 Ma. The zircon $\epsilon_{\text{Hf}}(t)$ ranges from +1.13 to +43.77, the t_{DM2} ranges from +655 to +1427 Ma, the initial Sr ratio ($^{87}\text{Sr}/^{86}\text{Sr}$)_i ranges from 0.7030 to 0.7036, and the $\epsilon_{\text{Nd}}(t)$ ranges from +2.1 to +6.6. Based on the geochemical compositions and isotopic characteristics of the rocks, the initial magma of the volcanic rocks in the Longjiang formation originated from the partial melting of basaltic crustal materials, with a source material inferred to be depleted mantle-derived young crustal. These rocks were formed in a superimposed post-collisional and continental arc environment, possibly associated with the Mongol–Okhotsk Ocean closure and the oblique subduction of the Pacific plate. This study addresses a research gap regarding the volcanic rocks of the Longjiang formation in this area. Its findings can be applied to exploration and prospecting in the region.



Citation: Wang, S.-C.; Hao, Y.-J.; Shi, L.; Tang, Z.; Zhu, S. Geochronology, Geochemical Characterization and Tectonic Background of Volcanic Rocks of the Longjiang Formation in the Lengjimanda Plate Area, Middle Da Hinggan Mountains. *Minerals* **2024**, *14*, 719. <https://doi.org/10.3390/min14070719>

Academic Editors: Aleksei V. Travin and Anastassia Yurievna Borisova

Received: 15 May 2024

Revised: 10 July 2024

Accepted: 11 July 2024

Published: 16 July 2024

Keywords: Longjiang volcanic rock; Da Hinggan mountains; zircon U–Pb dating; petro-geochemistry; Sr–Nd–Pb isotope; Lu–Hf isotope

1. Introduction

The Central Asian orogeny is a large Phanerozoic orogenic belt located between the North China, Tarim, and Siberian plates [1,2]. The Da Hinggan mountain region is situated in the eastern part of the Central Asian orogenic belt, between the Mongolia–Okhotsk suture line and the Xilamulun Yanji suture zone. It is a significant region, where the Paleozoic Paleo-Asian Oceanic metallogenetic tectonic domain is strongly superimposed, compounded, and transformed by the Mesozoic and Neo-Mesozoic Pacific metallogenetic tectonic domains [3–5]. The Paleozoic was characterized by the collision of small land masses and the closure of the Paleo-Asian Ocean [6,7], whereas the Mesozoic was characterized by the superposition and modification of the Paleo-Pacific plate and the Mongolian–Okhotsk plate [8,9]. Multiple phases of volcanic eruptions have resulted in



Copyright: © 2024 by the authors. Licensee MDPI, Basel, Switzerland. This article is an open access article distributed under the terms and conditions of the Creative Commons Attribution (CC BY) license (<https://creativecommons.org/licenses/by/4.0/>).

favorable metallogenic geological conditions in the area, with a variety of rock types [10] and extensive development of Mesozoic volcanic and granitic rocks [1,11]. The volcanic rocks are mainly Early Cretaceous rhyolite and basaltic andesite, distributed in facies-like formations [12]. The rock assemblage of the Mesozoic granites is primarily composed of granodiorite, monzogranite, and syenogranite, with a presence of A-type granites [13]. Several researchers have investigated the chronology and tectonic background of Mesozoic magmatism in the Da Hinggan mountains, and a basic understanding of the chronological framework delineation of different contemporaneous volcanic rocks has been achieved [14–16]; however, there are still some controversies regarding the tectonic background of these mountains, such as the subduction orogeny of the Ancient Pacific plate [17,18], and the post-orogenic extension in the Mongol-Okhotsk ocean [19,20]. Studies on the Da Hinggan mountains' Mesozoic stratigraphy have focused on the Tamulangou formation [21], Manketou Ebo formation [22], Manitou formation [23,24], and Baiyingaolao formation [25,26]. There are fewer studies on the Longjiang formation, and these studies do not provide a unified understanding of the era in which the Longjiang formation's volcanic rocks were formed [27,28]. Furthermore, these works mainly focused on the chronology and whole-rock geochemistry and lacked comprehensive studies of the Sr–Nd–Pb and Lu–Hf isotopes [29,30]. The strong stability of zircon minimizes the influence of later geological events on its Hf isotopic composition, while its extremely low Lu content allows us to accurately determine its Hf isotopic composition at the time of its formation. These properties make zircon an important tool for studying crustal evolution and tracing rock source regions [31–33]. Sr–Nd–Pb isotopic analyses are important in determining the petrogenesis of a formation, as they indicate the magma source and reveal the evolutionary pathways of rocks [34–37]. This study aimed to address the research gap concerning the volcanic rocks of the Longjiang formation. The objectives were to determine the formation age of the Longjiang formation's volcanic rocks, investigate their genesis and tectonic background, and reconstruct the geodynamic evolution of the region. This paper presents detailed petrological, zircon U–Pb geochronological, geochemical, and isotopic chemical analyses of the volcanic rocks of the Longjiang formation conducted through extensive field geological surveys using a geological map of the Lengjimanda plate at a scale of 1:25,000. The objective of this research is to provide reliable data for understanding the dynamic history of the Da Hinggan mountains.

2. Geological Background

The Lengjimanda plate area in the middle of the Da Hinggan mountains is located at the junction of the Xing'an block and the Songnen block in the eastern part of the Central Asian orogenic belt, which belongs to the Zhalantun Duobaoshan island arc (Figure 1a). During the Paleozoic, it was in the accretionary stage of the ancient Asian oceanic continental margin, forming an inland sedimentary basin. During the Mesozoic, it experienced the superposition, complexation, and transformation of the Paleo-Pacific tectonic domain and the Mongolian-Okhotsk oceanic tectonic domain [38], forming an inland volcanic basin [39]. In the Da Hinggan mountain region, the area was affected by the subduction of the Mongolian-Okhotsk oceanic plate during the Triassic. The study area experienced uplift and orogenic movements, resulting in the development of fragmented alteration or thrust faults in both the near-EW and near-NE directions [40]. During the Cretaceous, the area was influenced by the eastward subduction of the Paleo-Pacific plate towards the East Asian continent, forming volcanic rift basins and uplifts that were mainly distributed in the NNE direction. Due to the influence of multiple tectonic environments and superpositions, three main stages of structures developed in the study area. The first stage is characterized by NE reverse faults, the second stage by NNE shear zones, and the third stage by near-EW normal faults.

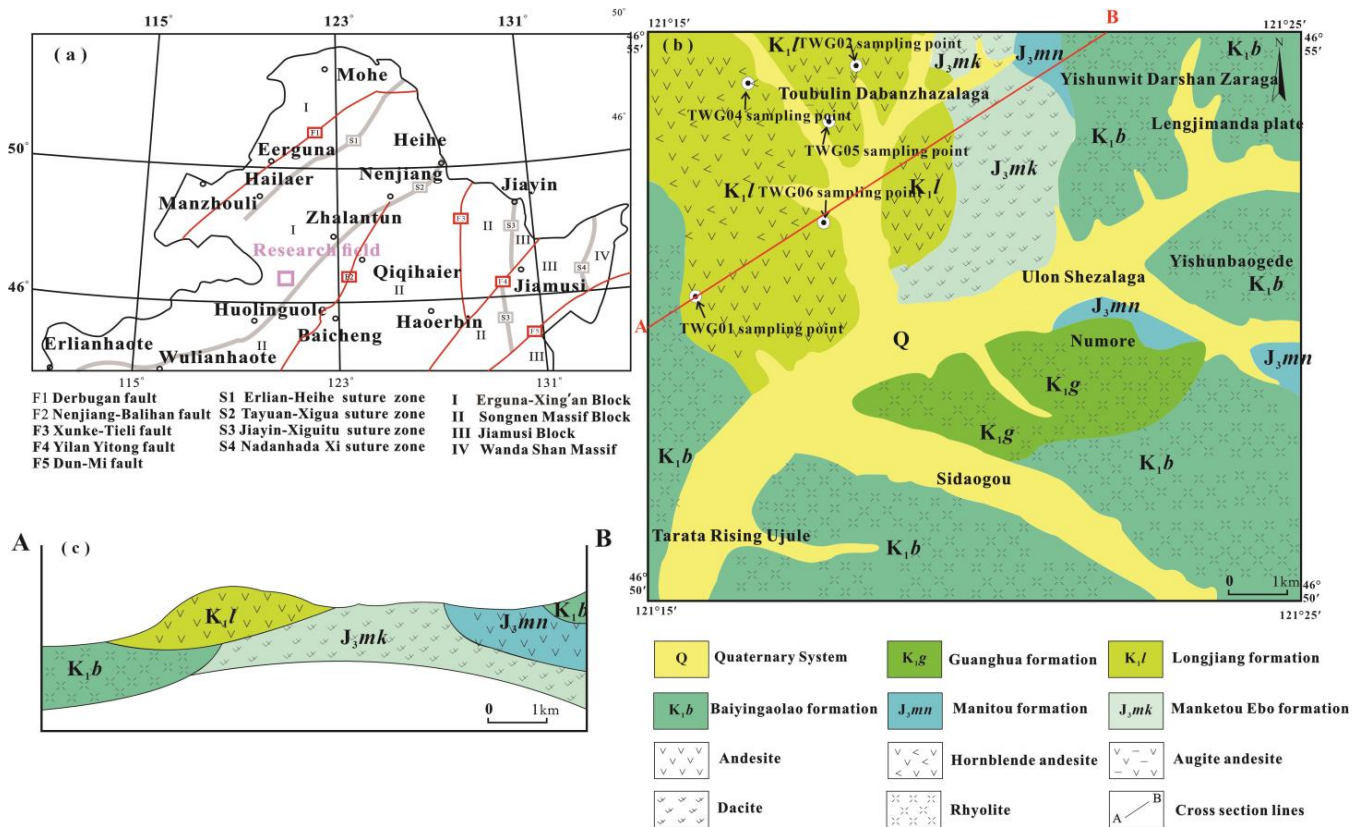


Figure 1. (a) The sample structural map in the Northeast region [40]; (b) plate geological map of LingjiManda plate, Da Hingan Mountains [41]; and (c) geological cross-section view of Lengjimanda plate.

The region is primarily characterized by Early Cretaceous intrusive rocks derived from the upper crust, with intrusion depths ranging from moderate to shallow. Several lithologies can be recognized, including granite quartz-bearing diorite, quartz-bearing monzonite, and granodiorite belonging to the high-potassium calc-alkaline series. Three types of vein rocks developed in the study area. They are mainly gray-black andesite, light pinkish-red syenite, and gray-white granite aplites. These three varieties occur together in the same location and have a NE distribution pattern, suggesting that they may have been formed by intrusion along a tectonic line.

The study area mainly consists of middle Jurassic Lower Cretaceous formations, which are the Wanbao formation (*J_{2wb}*), Manketou Ebo formation (*J_{3mk}*), Manitou formation (*J_{3mn}*), Baiyingaolao formation (*K_{1b}*), Longjiang formation (*K_{1l}*), and Guanghua formation (*K_{1g}*). The Longjiang formation is a suite of intermediate volcanic rocks characterized by different lithological types, including effusive basalt, explosive basaltic breccia tuff (comprising crystal and lithic fragments), volcanoclastic flow breccia tuff of a basaltic composition, and subvolcanic andesite. In the western part of the study area, particularly in the Tubulin Daban Zhalaga section, the Longjiang formation mainly consists of a suite of neutral to slightly alkaline volcanic rocks, with lithological assemblages including porphyritic rock, porphyritic andesite, andesite, andesitic brecciated tuff with angular lithic fragments, and locally developed andesitic volcanoclastic breccia (Figure 1b).

Sample TWG01 of the Longjiang formation was collected from the Toubulingda Zalaga area in the western part of Lengjimanda Banxi. The sampling coordinates are 46° 52'48" N, 121°15'36" E (Figure 2b). The weathered surface appears yellowish-brown, while the fresh surface is light gray. It exhibits a volcanic breccia structure with 30% angular clasts and 10% rock fragments composed of andesite. Crystals include 10% plagioclase and 20%

alkali feldspar. The volcanic glassy matrix is reddish-brown, flame-like, with 50% content, showing trachyandesite under indoor microscopic identification.

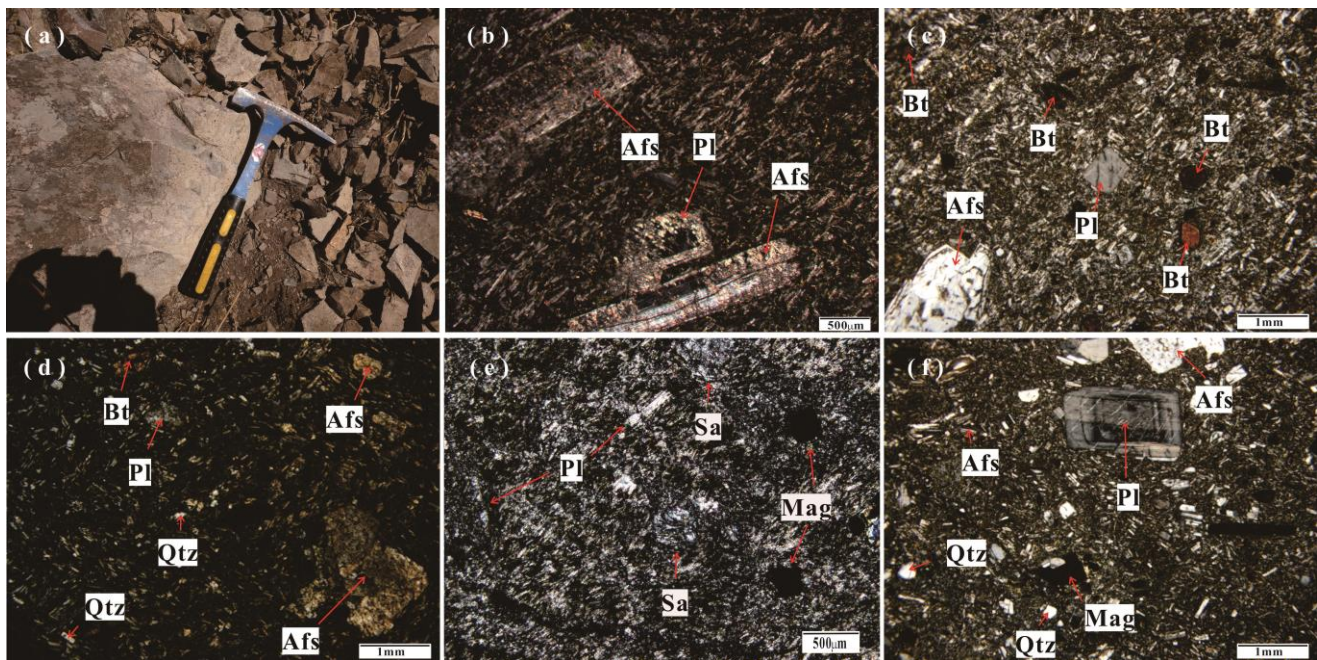


Figure 2. Hand specimen photo (a) and microscope photos (b–f) of the Lengjimanda plate. (a) TWG05; (b) TWG01; (c) TWG02; (d) TWG04; (e) TWG05; (f) TWG06, Sa: sanidine; Pl: plagioclase; Mag: magnetite; Afs: alkali feldspar; Bt: biotite; Qtz: quartz.

Sample TWG02 of the Longjiang formation was collected from the same area, with coordinates $46^{\circ} 54'36''$ N, $121^{\circ}17'24''$ E (Figure 2c). The weathered surface is yellowish-brown, and the fresh surface is light yellow with patchy structures and an interwoven matrix. The phenocrysts include 20% alkali feldspar, 10% plagioclase, and 5% biotite. The matrix has a microcrystalline interwoven structure of plagioclase, identified indoors as biotite trachyte rock.

Sample TWG04 of the Longjiang formation was collected nearby, with coordinates $46^{\circ} 53'59''$ N, $121^{\circ}50'11''$ E (Figure 2d). The weathered surface is light gray, and the fresh surface is dark gray with patchy structures and an interwoven matrix. Phenocrysts include 20% alkali feldspar, 10% plagioclase, and 5% biotite. The matrix has a microcrystalline interwoven structure of plagioclase, identified indoors as biotite trachyandesite.

Sample TWG05 of the Longjiang formation was collected with coordinates $46^{\circ}53'30''$ N, $121^{\circ}52'15''$ E (Figure 2e). The fresh surface is gray-brown with patchy and vesicular structures. Under polarized light microscopy, phenocrysts constitute approximately 5% to 10% of the sample, ranging from 2 to 4 mm in size, mainly composed of translucent feldspar and plagioclase. The feldspar phenocrysts exhibit tabular self-shaped structures, while the plagioclase phenocrysts are elongated tabular with semi- to self-shaped structures, some showing zoning. Phenocrysts and matrix display weak orientation, with the matrix predominantly glassy or cryptocrystalline, about 80%, occasionally showing fine needle-columnar plagioclase in microcrystalline interwoven structures.

Sample TWG06 of the Longjiang formation was collected with coordinates $46^{\circ} 53'21''$ N, $121^{\circ}52'18''$ E (Figure 2f). The weathered surface is yellowish-brown, and the fresh surface is dark gray with patchy structures and an interwoven matrix. Phenocrysts include 15% alkali feldspar, 20% plagioclase, and 2% magnetite. Alkali feldspar fills gaps between plagioclase microcrystals, identified indoors as trachyandesite.

3. Materials and Methods

The trachyandesite (TWG01, TWG04, and TWG06) and trachyte trachydacite (TWG02, TWG05) samples were picked up from the Toubulin-Dabanzhalaga area in the western part of the study area (Figure 1b). They were subjected to zircon LA-ICP-MS dating (except sample TWG02), whole rock major and trace element analyses, and Sr-Nb-Pb isotopic analyses (except sample TWG02). Zircon Lu-Hf isotope analyses were performed on a coarse-grained andesite sample (TWG01).

3.1. Major and Trace Element Analyses

Rock geochemical analysis was conducted at the Shenyang geological survey center, China geological survey. Fresh and unweathered samples were selected and then ground to a very fine power of about 80–200 μm for major and trace element analysis. A Rigaku Primus II X-ray fluorescence spectrometer (XRF-1500) was used for the determination of major element contents and analysis standards, according to Zhuo [42]. Chemical titration was used for the determination of FeO, and chemical mass analysis was used for the determination of loss on ignition, with analytical accuracy better than 1% to 5%. The trace and rare earth elements were determined using an Agilent 7500a inductively coupled plasma mass spectrometer (X-Series 2) with analytical accuracy better than 2% to 5%.

3.2. LA-ICP-MS Zircon U-Pb Dating

The separation, mounting, and microscopic image acquisition of zircon grains were conducted at the State Key Laboratory of Geological Processes and Mineral Resources at the Geosciences China University (Wuhan). First, samples were crushed to a particle size of 80–100 mesh using conventional methods. After magnetic and organic heavy liquid separations, zircon grains with consistent colors, crystal shapes, sizes, and low degrees of abrasion were selected. The selected zircon grains were then mounted on an epoxy resin, polished to half of their thickness, and coated with a gold film. The zircons selected from various samples exhibited morphological differences, including short prismatic and long prismatic shapes. Based on the CL images (Figure 3), zircons exhibiting the greatest degree of euhedry and oscillatory zoning, as well as the fewest inclusions, alterations, and cracks, were selected for experimentation. Zircon U-Pb dating was performed at the Qingdao National Laboratory for Marine Science and Technology, Chinese Academy of Sciences, using an Agilent 7500a LA-ICP-MS system coupled to a resolution M50 laser ablation system. The experiment employs helium as the carrier gas for the ablation material, and NIST 610 glass was used as the instrument monitoring standard. The age determination was calibrated using standard zircon 91500 and monitoring standard zircon Plešovice, and the laser spot diameter was 32 μm at a frequency of 7 Hz. The experimental procedures were like those described in Yuan [43]). Glitter software was used for signal selection, correction, and quantitative standardization of the experimental data, and ordinary Pb correction was performed using the method proposed by Andersen [44]. Age calculations and concordance plots were performed using Isoplot.

The measured age of the Plešovice zircon $^{206}\text{Pb}/^{238}\text{U}$ in the experiment was 342.21 ± 5.53 Ma, which is consistent with the standard value (337.13 ± 0.37 Ma; Sláma [45]) within the error range. The 91500 zircon $^{206}\text{Pb}/^{238}\text{U}$ age was 1062.44 ± 15.44 Ma, which is consistent with the standard value (1062.4 ± 0.8 Ma; Wiedenbeck [34]) within the error margin, indicating high accuracy and reliability.

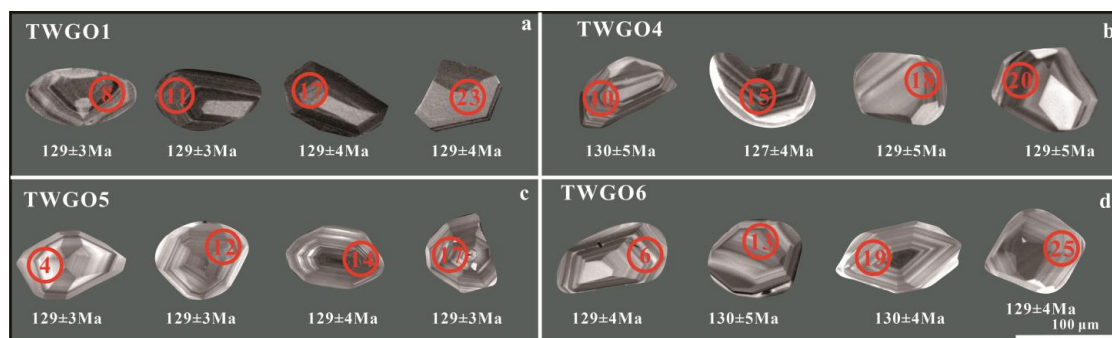


Figure 3. U–Pb zircons cathodoluminescence images from the volcanic rocks of the Longjiang formation at Lengjimanda plate. Circles indicate the locations of U–Pb analysis on zircons, along with their respective zircon numbers, and age information listed below. (a) TWG01, (b) TWG04, (c) TWG05, (d) TWG06.

3.3. The Sr–Nd–Pb Isotope Analysis

The pre-treatment and mass spectrometric determination of Sr–Nd–Pb isotopic analysis of volcanic rocks from the Longjiang formation were conducted at the State Key Laboratory for Mineral Deposits Research, Nanjing University, focusing on the ore-forming mechanisms of endogenous metal deposits. After dissolving the whole rock sample with a mixture of HF and HNO₃, AG50W × 8 cation exchange resin was used for the separation and purification of Sr and Nd using different eluents. For specific details of the procedure, please refer to Wei [46].

Sr–Nd isotopic analyses were performed using thermal ionization mass spectrometry (TIMS) on a solid isotope mass spectrometer. For the Sr isotope ratio determination, instrumental mass fractionation correction was performed using a reference value of $^{86}\text{Sr}/^{88}\text{Sr} = 0.1194$ with NIST SRM 987 as the external standard. For the Nd isotope analysis, the instrument mass fractionation correction was performed using a reference value of $^{146}\text{Nd}/^{144}\text{Nd} = 0.7219$ with the Nd isotope international standard material JNdi-1 as the external standard. The measurement accuracy was within 5 ppm for $^{143}\text{Nd}/^{144}\text{Nd}$ and within 10 ppm for $^{87}\text{Sr}/^{86}\text{Sr}$.

For Pb isotope analysis, the sample was dissolved in a mixture of HNO₃ and HF solutions in a volume ratio of 1:4. The Pb isotopes were then separated and purified using HBr and cation exchange resin. Pb isotopic testing and analysis were performed using thermal ionization mass spectrometry (TIMS), with instrumental mass fractionation correction using NIST Pb-981 and isotopic fractionation correction using NBS 981. The precision of the measurements was $^{206}\text{Pb}/^{204}\text{Pb} < 0.2\%$.

3.4. Zircon Lu–Hf Isotope Analysis

A micro-area Hf isotopic analysis was conducted on the samples based on the LA-ICP-MS zircon U–Pb isotopic analysis. Zircon Hf isotope analyses were performed at the State Key Laboratory for Mineral Deposits Research, Nanjing University. The experimental analysis used a Neptune MC–ICP–MS coupled with a COMPEX GeoLas Pro 193 nm ArF excimer laser ablation system. A laser spot diameter of 32 μm was used based on the size of the zircon grains, with a laser pulse frequency of 7 Hz. Helium was used as the ablation carrier gas. Zircon 91500 and MT were used as external reference materials. The obtained $^{176}\text{Hf}/^{177}\text{Hf}$ ratio was determined to be 0.282948 ± 0.000038 , which is within the error margin of the recommended value (0.282302 ± 8 ; Goolaerts [47]). Further details of the analytic procedure can be found in Wu [48].

4. Results

4.1. Major and Trace Element Compositions

The results of the major and trace element analyses of the volcanic rocks from the Longjiang formation are presented in Table 1.

Table 1. Major and trace element compositions of Lengjimanda plate of the Longjiang formation volcanic rocks.

Sample	TWG01YQ1	TWG01YQ2	TWG01YQ3	TWG01YQ4	TWG01YQ5	TWG02YQ1	TWG02YQ2	TWG02YQ3	TWG02YQ4	TWG02YQ5	TWG02YQ6	TWG04YQ1	TWG04YQ2
Lithology	Trachyandesite					Trachyte Trachydacite					Trachyandesite		
<i>Major elements (wt%)</i>													
SiO ₂	60.44	60.59	60.13	61.11	60.42	65.76	66.28	65.38	65.68	65.66	66.23	61.24	61.70
TiO ₂	1.09	1.09	1.11	1.09	1.07	0.63	0.60	0.62	0.59	0.62	0.61	0.84	0.83
Al ₂ O ₃	16.70	16.60	16.95	16.57	16.75	16.94	17.08	16.95	17.10	16.97	16.93	17.13	17.11
Fe ₂ O ₃ ^T	7.37	7.59	7.35	7.37	7.40	4.12	3.90	4.22	4.00	4.12	4.05	6.49	6.42
MnO	0.10	0.10	0.11	0.12	0.10	0.08	0.06	0.07	0.07	0.10	0.06	0.11	0.10
MgO	2.17	2.02	2.07	1.92	2.08	1.11	1.18	1.25	1.04	0.85	0.99	2.22	2.22
CaO	4.12	4.31	4.48	4.31	4.32	3.26	2.54	3.42	3.24	3.20	3.11	5.01	4.53
Na ₂ O	4.66	4.51	4.80	4.76	4.67	4.39	4.15	4.40	4.59	4.66	4.53	3.97	4.23
K ₂ O	2.99	2.85	2.63	2.42	2.86	3.55	4.04	3.52	3.51	3.62	3.37	2.92	2.77
P ₂ O ₅	2.99	2.85	2.63	2.42	2.86	3.55	4.04	3.52	3.51	3.62	3.37	2.92	2.77
LOI	1.63	1.39	1.63	1.54	1.42	2.08	2.46	1.48	1.43	1.73	1.66	1.58	1.39
Total	98.31	98.76	98.44	98.24	98.61	97.26	97.40	98.42	98.24	98.28	98.41	98.30	98.03
Na ₂ O/K ₂ O	1.56	1.58	1.82	1.96	1.63	1.24	1.03	1.25	1.31	1.29	1.34	1.36	1.53
A/NK	1.53	1.58	1.58	1.59	1.55	1.53	1.52	1.53	1.50	1.46	1.52	1.77	1.72
A/CNK	0.91	0.90	0.90	0.91	0.90	1.00	1.08	0.98	0.99	0.97	1.01	0.91	0.94
<i>Trace elements (ppm)</i>													
Sc	19.20	21.93	26.67	24.39	22.56	10.49	14.97	13.90	14.16	15.76	16.25	11.74	11.13
V	96.45	91.59	99.92	107.02	97.75	34.14	33.49	33.52	31.59	33.71	34.96	77.86	76.55
Cr	22.14	16.36	15.62	21.94	29.67	17.17	9.28	13.93	16.44	12.73	11.58	11.75	12.43
Co	27.50	27.90	30.65	27.42	30.30	11.91	12.92	12.19	12.99	10.98	12.03	17.59	16.50
Ni	19.70	19.47	22.90	20.40	23.87	12.20	12.03	13.22	13.78	11.87	18.08	5.98	3.79
Ga	23.28	23.44	22.20	23.31	22.84	20.05	20.58	21.64	20.34	20.47	20.75	18.47	18.59
Rb	61.53	62.45	61.01	54.50	61.37	90.81	107.72	93.00	97.73	95.13	88.03	72.54	69.80
Y	55.62	61.80	63.96	55.58	67.30	45.66	48.02	46.42	46.84	42.65	47.50	18.88	17.13
Zr	251.11	250.60	259.72	247.95	252.33	235.48	238.68	235.88	238.24	238.13	239.84	203.48	204.37
Nb	10.11	10.49	10.09	9.72	10.50	10.10	10.33	9.86	10.16	10.21	9.56	7.63	6.89
Ba	788.13	823.75	827.68	610.15	777.25	907.84	945.25	893.44	865.27	908.96	894.87	774.71	736.84
La	56.61	59.28	60.62	55.31	58.54	51.26	53.97	52.85	54.13	51.15	54.58	21.47	20.40
Ce	121.92	122.72	133.76	123.23	122.00	109.67	115.47	112.28	115.53	103.93	114.63	44.60	41.55
Nd	67.34	71.49	73.50	67.18	74.14	54.61	58.06	56.34	57.07	53.08	57.78	23.94	22.75
Sm	13.83	14.75	15.13	14.01	15.40	10.80	11.12	10.92	10.63	10.51	10.92	4.93	4.81
Eu	2.43	2.51	2.52	2.17	2.51	2.32	2.46	2.33	2.39	2.24	2.36	1.24	1.24

Table 1. Cont.

Sample	TWG01YQ1	TWG01YQ2	TWG01YQ3	TWG01YQ4	TWG01YQ5	TWG02YQ1	TWG02YQ2	TWG02YQ3	TWG02YQ4	TWG02YQ5	TWG02YQ6	TWG04YQ1	TWG04YQ2	
Lithology	Trachyandesite					Trachyte Trachydacite					Trachyandesite			
Gd	9.52	10.46	10.50	9.61	10.37	8.18	8.46	8.25	8.54	7.41	8.43	3.96	3.61	
Tb	0.93	0.98	1.02	0.90	1.04	0.73	0.75	0.73	0.76	0.75	0.75	0.53	0.53	
Dy	7.36	7.89	8.00	7.14	8.23	5.77	5.94	5.79	5.83	5.84	6.00	3.21	3.16	
Ho	1.08	1.20	1.17	1.08	1.13	0.87	0.89	0.88	0.87	0.81	0.89	0.63	0.57	
Er	3.35	3.61	3.62	3.38	3.59	2.76	2.95	2.89	2.97	2.58	2.93	2.03	2.00	
Tm	0.42	0.45	0.45	0.43	0.46	0.37	0.39	0.39	0.39	0.36	0.36	0.28	0.26	
Yb	2.84	3.02	3.26	2.92	3.02	2.51	2.59	2.67	2.55	2.56	2.60	1.83	1.83	
Lu	0.40	0.46	0.46	0.42	0.45	0.37	0.39	0.40	0.40	0.34	0.39	0.29	0.27	
Ta	0.98	0.99	1.15	1.02	1.15	1.20	1.07	1.07	0.95	1.08	1.15	0.54	0.38	
Th	5.06	4.82	5.01	4.56	4.85	4.56	5.16	5.40	5.60	6.82	4.74	7.15	6.72	
U	2.32	2.36	2.52	2.41	2.30	2.16	2.29	2.41	2.46	2.03	2.47	1.60	1.48	
ΣREE	304.68	316.19	331.91	304.35	319.59	264.42	278.26	271.12	276.64	255.04	277.41	114.82	108.51	
LREE	278.78	288.13	303.43	278.48	291.30	242.86	255.90	249.12	254.33	234.39	255.06	102.07	96.27	
HREE	25.90	28.06	28.48	25.87	28.29	21.56	22.36	22.00	22.31	20.65	22.35	12.75	12.24	
LREE/HREE	10.77	10.27	10.65	10.76	10.30	11.27	11.44	11.32	11.40	11.35	11.41	8.01	7.86	
La _N /Yb _N	14.31	14.08	13.35	13.59	13.89	14.68	14.92	14.18	15.23	14.31	15.05	8.42	8.00	
δEu	0.61	0.59	0.58	0.54	0.57	0.73	0.74	0.72	0.74	0.74	0.73	0.83	0.87	
δCe	0.96	0.93	0.98	0.99	0.90	0.98	0.98	0.98	0.99	0.95	0.97	0.96	0.94	
<i>Major elements (wt%)</i>														
SiO ₂	61.01	61.28	62.42	65.12	65.59	66.19	65.92	65.97	58.83	60.76	62.74	61.64	62.87	64.60
TiO ₂	0.85	0.83	0.82	0.61	0.58	0.55	0.56	0.58	0.88	0.88	0.83	0.84	0.81	0.79
Al ₂ O ₃	17.07	17.09	16.49	16.54	16.26	16.23	16.23	16.29	18.07	17.34	16.42	16.66	16.23	15.56
Fe ₂ O ₃ ^T	6.53	6.39	6.50	4.91	4.77	4.43	4.71	4.69	6.56	6.73	6.40	6.57	6.30	6.12
MnO	0.11	0.11	0.09	0.08	0.09	0.08	0.09	0.09	0.10	0.10	0.10	0.09	0.09	0.09
MgO	2.46	2.33	1.99	1.58	1.31	1.33	1.32	1.47	3.27	2.82	2.32	2.50	2.40	2.20
CaO	5.22	5.08	3.78	3.06	2.48	2.74	2.43	2.93	4.68	3.94	4.08	4.11	4.21	3.92
Na ₂ O	3.79	4.00	4.88	4.38	5.07	4.87	4.90	4.33	3.38	4.16	4.85	4.34	3.00	3.66
K ₂ O	2.89	2.87	2.93	3.70	3.86	3.55	3.80	3.63	3.95	3.04	2.05	3.02	3.82	2.87
P ₂ O ₅	2.89	2.87	2.93	3.70	3.86	3.55	3.80	3.63	3.95	3.04	2.05	3.02	3.82	2.87
LOI	1.48	1.32	1.57	1.51	1.45	1.55	1.49	1.68	3.34	2.47	1.94	2.37	3.04	2.58
Total	98.14	98.27	98.04	98.57	98.52	97.89	98.10	98.48	96.38	96.93	97.97	97.51	96.76	97.26
Na ₂ O/K ₂ O	1.31	1.39	1.66	1.18	1.32	1.37	1.29	1.19	0.86	1.37	2.37	1.44	0.79	1.28

Table 1. Cont.

Sample	TWG01YQ1	TWG01YQ2	TWG01YQ3	TWG01YQ4	TWG01YQ5	TWG02YQ1	TWG02YQ2	TWG02YQ3	TWG02YQ4	TWG02YQ5	TWG02YQ6	TWG04YQ1	TWG04YQ2	
Lithology	Trachyandesite					Trachyte Trachydacite					Trachyandesite			
A/NK	1.82	1.76	1.47	1.47	1.30	1.37	1.33	1.47	1.83	1.71	1.61	1.60	1.79	1.70
A/CNK	0.90	0.90	0.91	0.98	0.95	0.96	0.98	0.99	0.98	1.00	0.93	0.93	0.97	0.96
<i>Trace elements (ppm)</i>														
Sc	10.93	11.70	11.34	8.61	7.68	7.82	7.92	8.45	12.82	13.00	12.32	13.00	12.33	12.16
V	83.90	78.07	72.74	50.22	42.42	44.10	47.06	44.66	70.84	75.19	79.00	73.99	67.90	72.73
Cr	10.58	9.72	8.18	9.33	6.68	7.55	4.60	6.97	8.97	8.98	9.61	8.25	5.87	10.68
Co	15.25	16.36	15.20	10.76	9.22	9.84	9.69	9.92	17.42	18.16	16.67	17.38	16.94	16.25
Ni	4.87	4.10	3.04	0.85	0.12	1.61	0.66	0.22	4.58	4.52	3.82	4.00	3.91	4.00
Ga	18.61	19.24	17.81	17.63	17.54	17.75	19.43	17.34	18.49	18.50	16.45	16.71	15.09	16.75
Rb	70.28	70.83	73.37	98.83	97.18	91.25	99.49	95.51	88.08	71.83	40.45	70.13	88.08	67.41
Y	16.73	18.27	17.86	18.62	17.52	18.33	17.79	18.19	15.67	14.79	14.90	15.78	15.66	14.28
Zr	201.17	200.88	191.20	258.32	272.94	272.23	273.57	269.53	192.03	193.80	184.57	182.28	175.72	168.28
Nb	6.84	6.50	7.07	8.31	8.75	8.92	8.20	7.92	6.78	6.77	6.90	7.37	6.53	6.90
Ba	676.71	698.50	795.31	932.24	1000.00	1000.00	959.58	961.40	1100.00	866.52	741.55	808.76	110.00	732.53
La	19.32	20.50	20.55	23.03	22.45	23.82	23.41	23.46	20.52	20.16	19.88	20.24	19.21	19.49
Ce	40.38	43.01	42.20	46.33	47.94	48.45	47.40	48.49	43.54	42.19	41.22	42.74	40.82	40.42
Nd	21.79	23.46	23.06	23.48	23.08	23.61	23.25	23.61	23.28	23.36	22.18	23.21	22.28	21.79
Sm	4.37	4.86	4.64	4.48	4.52	4.54	4.52	4.49	4.74	4.57	4.55	4.65	4.60	4.24
Eu	1.16	1.08	1.20	1.15	1.13	1.17	1.08	1.10	1.19	1.24	1.17	1.11	1.02	1.11
Gd	3.62	3.83	3.75	3.63	3.55	3.56	3.46	3.53	3.77	3.55	3.64	3.72	3.62	3.45
Tb	0.49	0.54	0.53	0.50	0.51	0.50	0.50	0.50	0.52	0.49	0.50	0.52	0.50	0.46
Dy	2.88	3.10	3.10	3.04	3.02	2.97	2.92	2.90	2.86	2.98	2.71	2.85	2.76	2.58
Ho	0.56	0.60	0.61	0.60	0.55	0.60	0.56	0.59	0.53	0.49	0.50	0.52	0.52	0.47
Er	1.87	2.00	1.98	2.02	1.97	2.00	2.00	2.01	1.67	1.57	1.56	1.65	1.63	1.51
Tm	0.26	0.28	0.27	0.29	0.30	0.29	0.28	0.30	0.22	0.19	0.21	0.21	0.22	0.19
Yb	1.72	1.84	1.83	1.98	1.98	2.03	1.89	1.98	1.39	1.25	1.29	1.34	1.35	1.23
Lu	0.26	0.28	0.28	0.31	0.29	0.32	0.30	0.31	0.20	0.18	0.18	0.19	0.19	0.17
Ta	0.35	0.51	0.46	0.47	0.48	0.70	0.38	0.42	0.40	0.41	0.34	0.38	0.33	0.27
Th	6.21	6.35	6.44	7.62	8.53	8.17	8.22	8.17	4.62	4.11	3.77	4.30	4.19	4.07
U	1.51	1.58	1.47	1.85	1.90	1.99	1.91	1.99	1.38	1.18	1.48	1.43	1.46	1.17
ΣREE	103.99	111.17	109.72	116.90	117.05	119.99	117.61	119.36	110.18	108.21	105.04	108.57	104.15	102.47
LREE	92.34	98.68	97.36	104.52	104.89	107.71	105.69	107.25	99.03	97.51	94.46	97.58	93.37	92.41
HREE	11.66	12.49	12.36	12.38	12.16	12.28	11.92	12.11	11.16	10.70	10.58	10.99	10.78	10.06

Table 1. Cont.

Sample	TWG01YQ1	TWG01YQ2	TWG01YQ3	TWG01YQ4	TWG01YQ5	TWG02YQ1	TWG02YQ2	TWG02YQ3	TWG02YQ4	TWG02YQ5	TWG02YQ6	TWG04YQ1	TWG04YQ2	
Lithology	Trachyandesite					Trachyte Trachydacite					Trachyandesite			
LREE/HREE	7.92	7.90	7.88	8.44	8.62	8.77	8.87	8.86	8.88	9.11	8.93	8.87	8.66	9.19
La _N /Yb _N	8.05	7.98	8.06	8.33	8.15	8.42	8.89	8.52	10.58	11.53	11.04	10.86	10.22	11.35
δEu	0.86	0.74	0.85	0.84	0.83	0.86	0.80	0.82	0.83	0.91	0.85	0.79	0.74	0.86
δCe	0.96	0.95	0.94	0.94	1.01	0.96	0.95	0.97	0.97	0.93	0.95	0.97	0.96	0.95

The SiO₂ content of the volcanic rock samples from the Longjiang formation ranges from 58.83% to 66.28%, with an average of 63.17%. The total alkali content (Na₂O+K₂O) ranges from 6.50% to 8.80%, with an average of 7.29%. In the N₂O+K₂O-SiO₂ diagram (Figure 4), the samples' chemical compositions fall into the fields of trachyandesite, trachyte trachydacite, andesite, and dacite; in the SiO₂ vs. K₂O diagram (Figure 5a), the samples mainly fall into the calc-alkaline to high-K calc-alkaline series. The aluminum-rich Al₂O₃ content ranges from 15.26% to 18.07%, with an average of 16.75%. The aluminum saturation index A/CNK ranges from 0.90 to 1.08, with an average of 0.95. In the A/NK-A/CNK diagram (Figure 5b), the sample's chemical composition mainly falls into the sub-aluminous rock category; the TiO₂ content ranges from 0.55% to 1.11%, with an average of 0.79%. The Fe₂O₃^T content ranges from 4.00% to 7.37%, with an average of 5.78%. The MgO content ranges from 0.85% to 3.27%, with an average of 1.87%. The Mg[#] content ranges from 28.75 to 50.32, with an average of 37.85. The CaO content ranges from 2.43% to 5.08%, with an average of 3.80%. The Thorpe index σ ranges from 1.56 to 3.65, with an average of 2.96. These values indicate that the volcanic rocks of the Longjiang formation in the Lengjimanda plate are a series of intermediate basic volcanic rocks belonging to the calc-alkaline series.

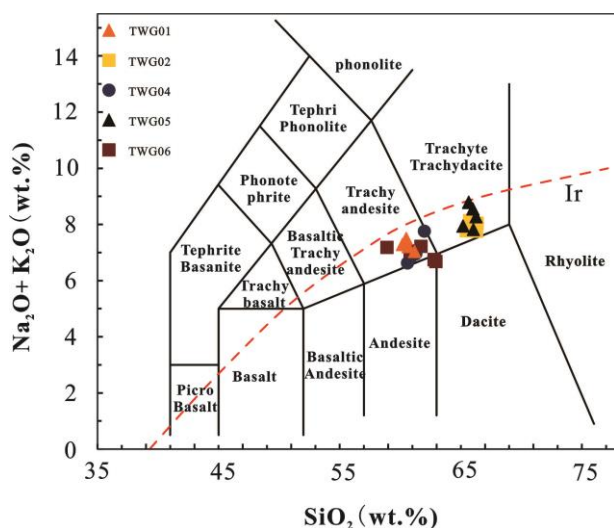


Figure 4. Diagram of (N₂O+K₂O) vs. SiO₂ of volcanic rocks of Longjiang formation [49].

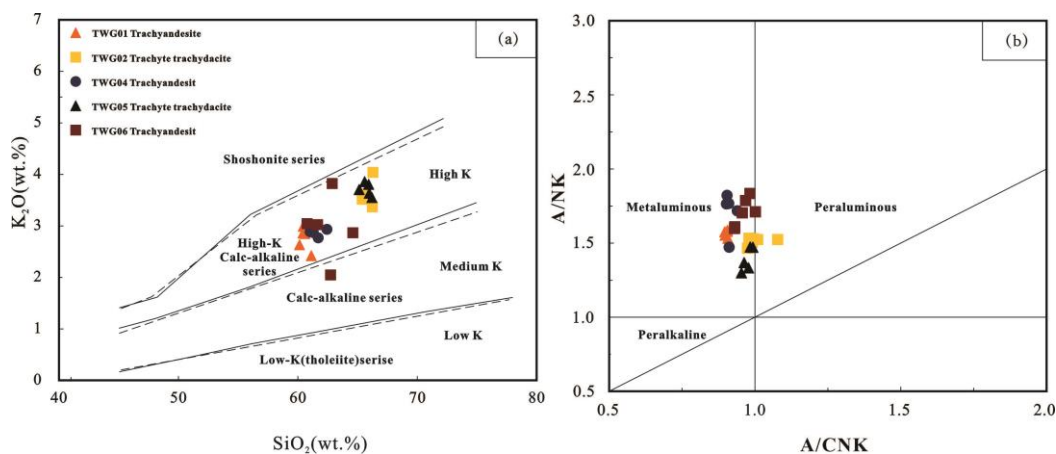


Figure 5. Major elements classification diagrams of Longjiang formation volcanic rocks, Lengjimanda plate. (a) K₂O vs. SiO₂ diagram [50]; (b) A/NK vs. A/CNK diagram [50].

These volcanic rocks are relatively enriched in large-ion lithophile elements (such as Rb, K, Ba, U, and LREE) and depleted in high-field-strength elements (such as Nb, Ta, Zr,

Hf, and HREE). The Rb/Sr values range from 0.09 to 0.19, with an average of 0.13 (Figure 6), which is higher than the Rb/Sr values of the primitive mantle (0.03), E-MORB (0.033), and OIB (0.047), but lower than those of the crustal source magma (>0.5). The Th/Pb values range from 1.9 to 5.3, with an average of 3.17, which is between those of the crustal source rocks and the primitive mantle. The Nb/Ta values range from 8.33 to 26.03, with an average of 14.51, which is also between those of the crustal source rocks and the primitive mantle. The rocks are characterized by high Sr (average 634.22 ppm), low Y (average 31.55 ppm), low Yb (average 2.12 ppm), and high Sr/Y (average 27.59) values.

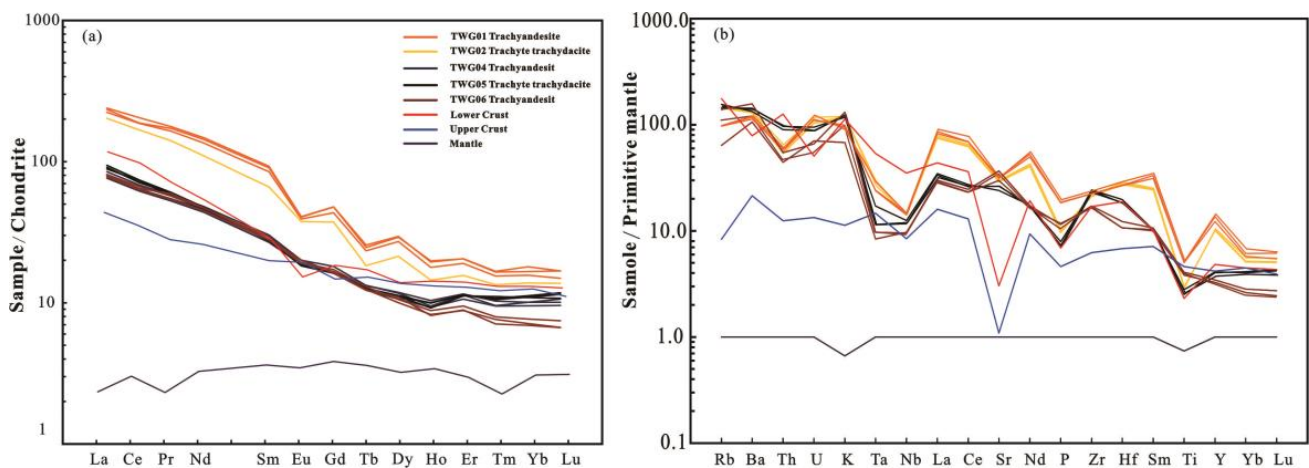


Figure 6. (a) Chondrite-normalized REE distribution patterns [51] and (b) primitive mantle-normalized spider diagrams [52] of the Longjiang formation volcanic rocks, Lengjimanda plate.

The total rare earth element content of these volcanic rocks from the Longjiang formation ranges from 56.23 ppm to 331.91 ppm, with an average of 184.35 ppm. The light rare earth element content ranges from 92.41 ppm to 333.91 ppm, with an average of 167.52 ppm, while the heavy rare earth element content ranges from 10.06 ppm to 28.48 ppm, with an average of 16.83 ppm. The LREE/HREE ratio ranges from 7.86 to 11.44, with an average of 9.55. The enrichment of light REEs and depletion of heavy REEs are indicated by the right-skewed distribution of REE patterns when they are normalized to chondrite (Figure 6). The fractionation of light and heavy REE is evident, with the fractionation coefficients $(La/Yb)_N$ ranging from 7.98 to 15.23, with an average of 11.33. The δEu values range from 0.54 to 1.19, and except for a few samples with positive Eu anomalies, most samples show moderately negative Eu anomalies.

4.2. Zircon U–Pb Isotopic Dating

The results of the zircon U–Pb isotopic analyses of the volcanic rock samples from the Longjiang formation are shown in Table 2.

The ^{232}Th content ranges from 44 ppm to 1126 ppm, while the ^{238}U content ranges from 70 ppm to 1157 ppm. The $^{232}\text{Th}/^{238}\text{U}$ ratio ranges from 0.199 to 1.711. Based on the characteristics observed in the CL images (Figure 3), it is suggested that these zircons are magmatic (Supplementary Materials).

Of the 30 analyzed points on the trachyandesite (TGW01), 27 measurement spots show good age consistency, except for 5 zircon grains with significant age anomalies. In the concordance plot of the zircon U–Pb ages (Figure 7a), all the obtained zircon U–Pb ages lie along or near the concordance line after discordant points are excluded. The $^{206}\text{Pb}/^{238}\text{U}$ weighted mean age is 129.1 ± 0.65 Ma (MSWD = 0.93, $n = 27$), indicating an Early Cretaceous age.

Table 2. Zircon LA-ICP-MS U-Pb data of the volcanic rocks from Lengjimanda plate of the Longjiang formation.

Sample	Lithology	Concentration (ppm)			Ratio						Age/Ma			
		²³² Th	²³⁸ U	Th/U	²⁰⁷ Pb/ ²⁰⁶ Pb	±%	²⁰⁷ Pb/ ²³⁵ U	±%	²⁰⁶ Pb/ ²³⁸ U	±%	²⁰⁷ Pb/ ²³⁵ U	2σ	²⁰⁶ Pb/ ²³⁸ U	2σ
TWG01-01		46	70	0.657	0.04751	0.00484	0.14564	0.01571	0.0203	0.00064	138	14	130	4
TWG01-02		208	591	0.352	0.05698	0.00229	0.15885	0.00687	0.02023	0.0005	150	6	129	3
TWG01-03		225	593	0.379	0.05458	0.00237	0.14969	0.00697	0.02021	0.0005	142	6	129	3
TWG01-04		185	351	0.529	0.04789	0.0021	0.13013	0.00608	0.0202	0.0005	124	5	129	3
TWG01-05		260	296	0.878	0.05145	0.00257	0.1447	0.00771	0.02035	0.00052	137	7	130	3
TWG01-06		222	301	0.738	0.04909	0.00281	0.129	0.00781	0.02021	0.00053	123	7	129	3
TWG01-07		775	453	1.711	0.05501	0.00228	0.15136	0.00675	0.02024	0.0005	143	6	129	3
TWG01-08		123	147	0.834	0.05014	0.00297	0.1356	0.00852	0.02018	0.00053	129	8	129	3
TWG01-09		57	80	0.71	0.07026	0.01095	0.19627	0.03278	0.02025	0.00093	182	28	129	6
TWG01-10		202	232	0.87	0.04973	0.00259	0.13746	0.00764	0.02034	0.00052	131	7	130	3
TWG01-11		98	215	0.459	0.04682	0.00326	0.13114	0.00965	0.02024	0.00055	125	9	129	3
TWG01-12		110	155	0.712	0.05788	0.00384	0.15738	0.01111	0.02021	0.00056	148	10	129	4
TWG01-13		111	107	1.034	0.04724	0.00334	0.13109	0.00979	0.0202	0.00055	125	9	129	4
TWG01-14		57	105	0.545	0.04748	0.00319	0.13425	0.00956	0.02021	0.00055	128	9	129	3
TWG01-15	Trachyandesite	251	626	0.401	0.04927	0.00169	0.13916	0.00521	0.02026	0.00049	132	5	129	3
TWG01-16		196	256	0.766	0.05052	0.00249	0.14164	0.00747	0.02022	0.00051	135	7	129	3
TWG01-17		46	99	0.466	0.04704	0.00382	0.13702	0.01175	0.02025	0.00058	130	10	129	4
TWG01-18		422	789	0.535	0.04594	0.00153	0.13004	0.00474	0.02023	0.00049	124	4	129	3
TWG01-19		43	64	0.679	0.04992	0.00448	0.14338	0.01359	0.02024	0.00061	136	12	129	4
TWG01-20		159	213	0.744	0.05181	0.00261	0.14772	0.00797	0.02019	0.00051	140	7	129	3
TWG01-21		265	373	0.71	0.04994	0.00209	0.14159	0.00643	0.02023	0.0005	135	6	129	3
TWG01-22		618	1157	0.534	0.05277	0.00154	0.15015	0.00491	0.02023	0.00048	142	4	129	3
TWG01-23		59	99	0.6	0.04949	0.00361	0.13722	0.01061	0.02025	0.00056	131	9	129	4
TWG01-24		203	259	0.783	0.04776	0.00631	0.14546	0.02029	0.02011	0.00073	138	18	128	5
TWG01-25	125	157	0.798	0.05601	0.0043	0.17888	0.01475	0.02028	0.00059	167	13	130	4	
TWG01-26	50	77	0.647	0.04413	0.00482	0.12089	0.01383	0.02018	0.00065	116	13	129	4	
TWG01-27	181	253	0.716	0.05329	0.00277	0.14754	0.00825	0.02023	0.00052	140	7	129	3	
TWG01-28	181	192	0.943	0.04598	0.00519	0.13447	0.01598	0.02016	0.00067	128	14	129	4	
TWG01-29	105	116	0.912	0.05187	0.00365	0.1547	0.0116	0.0202	0.00056	146	10	129	4	
TWG01-30	242	205	1.185	0.06303	0.00427	0.18018	0.01313	0.02016	0.00057	168	11	129	4	

Table 2. Cont.

Sample	Lithology	Concentration (ppm)			Ratio						Age/Ma			
		²³² Th	²³⁸ U	Th/U	²⁰⁷ Pb/ ²⁰⁶ Pb	±%	²⁰⁷ Pb/ ²³⁵ U	±%	²⁰⁶ Pb/ ²³⁸ U	±%	²⁰⁷ Pb/ ²³⁵ U	2σ	²⁰⁶ Pb/ ²³⁸ U	2σ
TWG04-1	Trachyandesite	44	48	0.922	0.15379	0.00562	8.12828	0.32538	0.38309	0.01152	2245	36	2091	54
TWG04-2		706	949	0.744	0.05827	0.00192	0.48677	0.01815	0.06055	0.00169	403	12	379	10
TWG04-3		882	1118	0.789	0.04837	0.00227	0.13442	0.00669	0.02014	0.00058	128	6	129	4
TWG04-4		124	222	0.56	0.05296	0.00429	0.14817	0.01207	0.02028	0.00065	140	11	129	4
TWG04-5		545	829	0.657	0.04985	0.00237	0.13901	0.00699	0.02021	0.00058	132	6	129	4
TWG04-6		180	264	0.683	0.05155	0.0039	0.14345	0.01095	0.02018	0.00064	136	10	129	4
TWG04-7		506	856	0.591	0.05584	0.00246	0.1561	0.00735	0.02027	0.00058	147	6	129	4
TWG04-8		413	479	0.862	0.05517	0.00266	0.15355	0.00781	0.02018	0.00059	145	7	129	4
TWG04-9		132	192	0.684	0.05611	0.00546	0.15638	0.01514	0.02021	0.00071	148	13	129	4
TWG04-10		335	343	0.976	0.0505	0.00575	0.14168	0.01599	0.02034	0.00074	135	14	130	5
TWG04-11		150	348	0.431	0.22667	0.00849	1.1992	0.04775	0.03836	0.00118	800	22	243	7
TWG04-12		304	390	0.777	0.0489	0.00519	0.13624	0.01438	0.0202	0.00071	130	13	129	5
TWG04-13		507	850	0.597	0.05193	0.0028	0.14567	0.00819	0.02035	0.00061	138	7	130	4
TWG04-14		478	761	0.629	0.04914	0.00317	0.13669	0.00903	0.02018	0.00062	130	8	129	4
TWG04-15		784	1083	0.724	0.05212	0.00283	0.14269	0.00807	0.01987	0.0006	135	7	127	4
TWG04-16		112	123	0.911	0.05116	0.00744	0.14163	0.02033	0.02009	0.00083	135	18	128	5
TWG04-17		134	201	0.667	0.05667	0.00509	0.15692	0.01409	0.0201	0.00069	148	12	128	4
TWG04-18		340	417	0.815	0.06105	0.00598	0.17061	0.01661	0.02028	0.00073	160	14	129	5
TWG04-19		390	686	0.568	0.04551	0.00291	0.12634	0.00831	0.02015	0.00062	121	7	129	4
TWG04-20		95	154	0.621	0.0586	0.00676	0.16277	0.01855	0.02016	0.00078	16	129	5	146
TWG05-1	Trachyte Trachydacite	80	121	0.661	0.05421	0.00451	0.15118	0.01256	0.02022	0.00063	143	11	129	4
TWG05-2		103	178	0.578	0.05556	0.00324	0.15484	0.00913	0.02021	0.00056	146	8	129	4
TWG05-3		316	371	0.852	0.04549	0.00222	0.12682	0.00636	0.02022	0.00054	121	6	129	3
TWG05-4		232	343	0.678	0.04889	0.00233	0.13639	0.00669	0.02023	0.00054	130	6	129	3
TWG05-5		213	316	0.673	0.05233	0.00253	0.1459	0.00724	0.02022	0.00054	138	6	129	3
TWG05-6		128	215	0.595	0.05284	0.00312	0.14831	0.00883	0.02035	0.00057	140	8	130	4
TWG05-7		188	269	0.702	0.04665	0.00245	0.12989	0.00697	0.02019	0.00054	124	6	129	3
TWG05-8		127	168	0.756	0.06221	0.00303	0.1735	0.00862	0.02023	0.00054	163	7	129	3
TWG05-9		112	155	0.723	0.04756	0.00439	0.13178	0.01207	0.0201	0.00062	126	11	128	4
TWG05-10		77	168	0.459	0.0515	0.00393	0.14361	0.01092	0.02022	0.00059	136	10	129	4

Table 2. Cont.

Sample	Lithology	Concentration (ppm)			Ratio						Age/Ma			
		²³² Th	²³⁸ U	Th/U	²⁰⁷ Pb/ ²⁰⁶ Pb	±%	²⁰⁷ Pb/ ²³⁵ U	±%	²⁰⁶ Pb/ ²³⁸ U	±%	²⁰⁷ Pb/ ²³⁵ U	2σ	²⁰⁶ Pb/ ²³⁸ U	2σ
TWG05-11	Trachyte Trachydacite	113	157	0.72	0.06375	0.00394	0.17798	0.01101	0.02025	0.00057	166	9	129	4
TWG05-12		267	354	0.757	0.04806	0.0021	0.13436	0.00607	0.02028	0.00052	128	5	129	3
TWG05-13		180	299	0.602	0.0542	0.00275	0.15163	0.00783	0.02029	0.00054	143	7	130	3
TWG05-14		101	145	0.696	0.05973	0.00405	0.16683	0.0113	0.02026	0.00057	157	10	129	4
TWG05-15		330	406	0.812	0.04791	0.00215	0.13301	0.00612	0.02014	0.00051	127	5	129	3
TWG05-16		80	172	0.465	0.06122	0.0034	0.17024	0.00949	0.02017	0.00054	160	8	129	3
TWG05-17		179	272	0.658	0.07161	0.00372	0.20022	0.01046	0.02028	0.00055	185	9	129	3
TWG05-18		70	132	0.534	0.05234	0.00473	0.14607	0.01306	0.02025	0.00062	138	12	129	4
TWG05-19		122	241	0.505	0.05364	0.00339	0.14898	0.00942	0.02015	0.00055	141	8	129	4
TWG05-20		182	303	0.602	0.05304	0.00261	0.14746	0.00737	0.02017	0.00052	140	7	129	3
TWG06-1	Trachyandesite	73	145	0.504	0.05341	0.00588	0.14797	0.0161	0.02009	0.0007	140	14	128	4
TWG06-2		62	131	0.474	0.05027	0.00566	0.14041	0.01565	0.02026	0.0007	133	14	129	4
TWG06-3		182	277	0.658	0.0509	0.00364	0.14292	0.01028	0.02036	0.00061	136	9	130	4
TWG06-4		80	141	0.569	0.0582	0.00368	0.1628	0.0104	0.02028	0.00059	153	9	130	4
TWG06-5		71	133	0.531	0.04539	0.00491	0.12732	0.01368	0.02034	0.00067	122	12	130	4
TWG06-6		97	156	0.622	0.04747	0.00462	0.13202	0.01278	0.02017	0.00065	126	11	129	4
TWG06-7		164	227	0.723	0.06413	0.00441	0.17815	0.01228	0.02015	0.00061	167	11	129	4
TWG06-8		85	118	0.726	0.04662	0.00479	0.12975	0.01323	0.02018	0.00066	124	12	129	4
TWG06-9		451	503	0.896	0.0542	0.003	0.15143	0.00856	0.02026	0.00057	143	8	129	4
TWG06-10		416	432	0.962	0.06778	0.0026	0.18953	0.00772	0.02028	0.00055	176	7	129	3
TWG06-11		311	320	0.972	0.05628	0.00432	0.1572	0.01205	0.02026	0.00062	148	11	129	4
TWG06-12		967	677	1.43	0.05893	0.00216	0.16419	0.00645	0.02021	0.00054	154	6	129	3
TWG06-13		85	149	0.57	0.03933	0.00583	0.11011	0.01614	0.02031	0.00076	106	15	130	5
TWG06-14		253	291	0.868	0.09994	0.00652	0.27891	0.01801	0.02024	0.00064	250	14	129	4
TWG06-15		307	373	0.823	0.04796	0.00401	0.13424	0.0112	0.0203	0.00063	128	10	130	4
TWG06-16		189	351	0.539	0.04445	0.00469	0.12308	0.01287	0.02008	0.00067	118	12	128	4
TWG06-17		289	423	0.684	0.05073	0.00281	0.14148	0.00798	0.02022	0.00057	134	7	129	4
TWG06-18		80	135	0.593	0.0475	0.00508	0.13168	0.01397	0.0201	0.00068	126	13	128	4
TWG06-19		64	123	0.519	0.05107	0.00496	0.14296	0.01379	0.0203	0.00066	136	12	130	4
TWG06-20		104	156	0.666	0.05726	0.00496	0.15965	0.01373	0.02022	0.00065	150	12	129	4
TWG06-21		179	220	0.815	0.05182	0.00355	0.14473	0.00997	0.02025	0.00059	137	9	129	4
TWG06-22		75	149	0.504	0.06617	0.00556	0.18432	0.01533	0.0202	0.00066	172	13	129	4
TWG06-23		122	189	0.648	0.05238	0.00394	0.14676	0.01104	0.02032	0.00061	139	10	130	4
TWG06-24		141	162	0.87	0.05283	0.00505	0.14759	0.01396	0.02026	0.00067	140	12	129	4
TWG06-25		265	360	0.735	0.04851	0.00283	0.13479	0.008	0.02015	0.00056	128	7	129	4

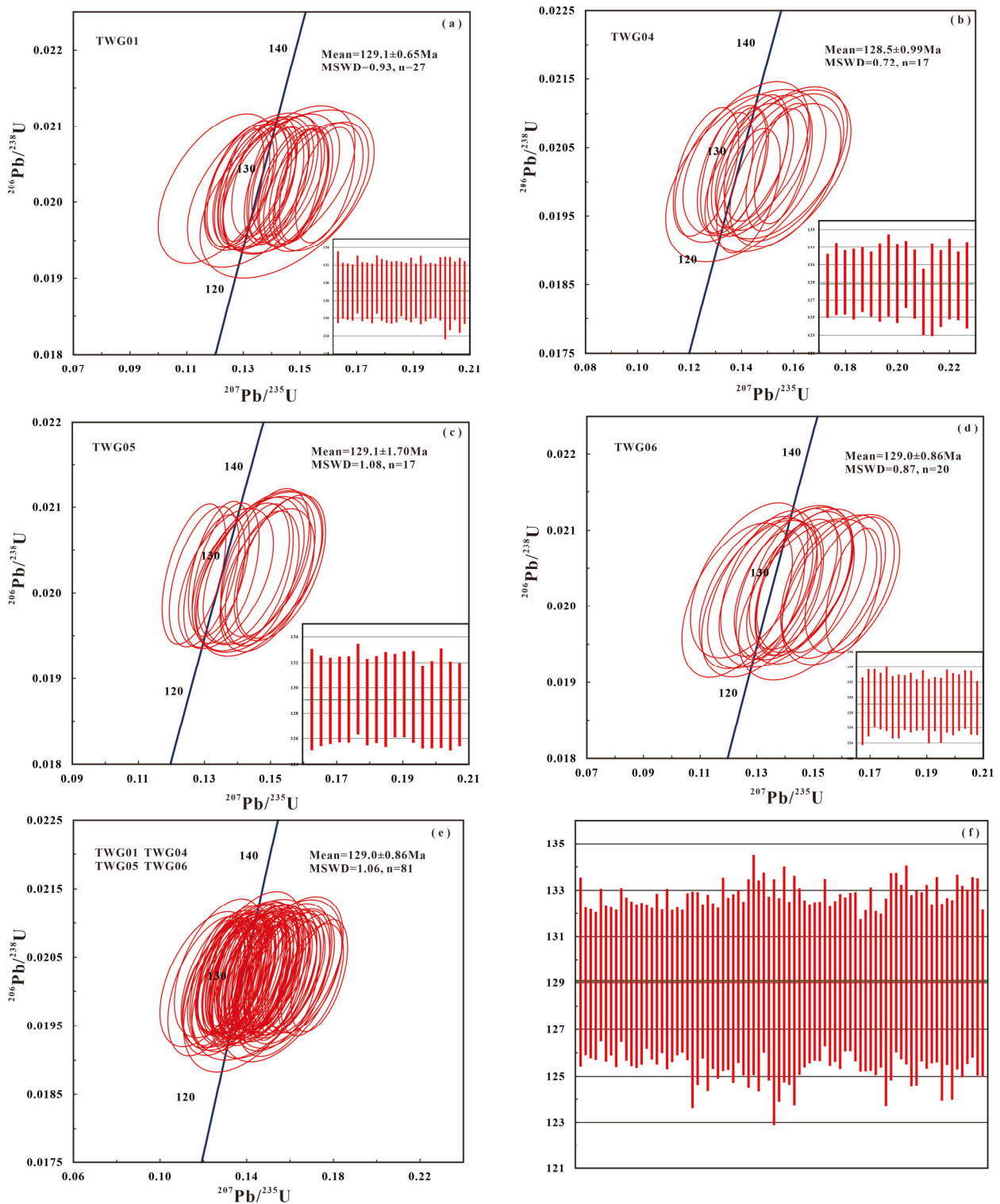


Figure 7. Concordant and weighted diagrams of the zircon U-Pb age of the Longjiang formation volcanic rocks, Lengjimanda plate. Error ellipses are shown for 1-sigma level of uncertainty. (a) TWG01, (b) TWG04, (c) TWG05, (d) TWG06, (e) Longjiang formation volcanic rocks, (f) weighted diagrams of the Longjiang formation volcanic rocks.

Of the 20 analyzed points in the trachyandesite sample (TWG04), 17 measurement spots show good age consistency. In the concordance plot of the zircon U-Pb ages (Figure 7b), all the obtained zircon U-Pb ages lie on or near the concordance line after discor-

dant points have been excluded. The weighted mean age of $^{206}\text{Pb}/^{238}\text{U}$ is 128.5 ± 0.99 Ma (MSWD = 0.72, $n = 17$), indicating an Early Cretaceous age.

Of the 20 analyzed points in the trachyte trachydacite sample (TWG05), 17 zircon measurement points show good age consistency. In the concordance plot of the zircon U–Pb ages (Figure 7c), all the obtained zircon U–Pb ages lie on or near the concordance line after discordant points are excluded. The weighted mean age of $^{206}\text{Pb}/^{238}\text{U}$ is determined to be 129.1 ± 1.70 Ma (MSWD = 1.08, $n = 17$), indicating an Early Cretaceous age.

Of the 25 analyzed points in the trachyandesite sample (TWG06), 20 zircon measurement points show good age consistency. In the concordance plot of the zircon U–Pb ages (Figure 7d), all the obtained zircon U–Pb ages lie on or near the concordance line after discordant points are excluded. The weighted mean age of $^{206}\text{Pb}/^{238}\text{U}$ is determined to be 129.0 ± 0.86 Ma (MSWD = 0.87, $n = 20$), indicating an Early Cretaceous age.

The volcanic rock samples from various sampling locations in the Longjiang formation have a total of 95 analytical points. Among them, 14 spots show significant deviations in their zircon surface ages due to poor separation and a complex composition, while the remaining 81 spots show good age consistency. In the concordance plot of the zircon U–Pb ages (Figure 7f), all the obtained zircon U–Pb ages lie along or near the concordance line after discordant points are excluded. The weighted mean age of $^{206}\text{Pb}/^{238}\text{U}$ is determined to be 129.0 ± 0.86 Ma (MSWD = 1.06, $n = 81$), indicating an Early Cretaceous age.

4.3. Sr–Nd–Pb Isotopic Dating

The Sr–Nd–Pb isotopic compositions of the volcanic rocks of Longjiang formation volcanic rocks are shown in Table 3. The initial Sr and Nd isotopic compositions of the samples in the study area are corrected based on their corresponding zircon U–Pb ages of 129 Ma.

Table 3. Sr–Nd–Pb isotopic data of the Longjiang formation volcanic rocks.

Sample	Age Ma	Rb ppm	Sr	$^{87}\text{Rb}/$ ^{86}Sr	$(^{87}\text{Sr}/$ $^{86}\text{Sr})_i$	Sm	Nd	$^{147}\text{Sm}/$ ^{144}Nd	$^{143}\text{Nd}/$ ^{144}Nd	$(^{143}\text{Nd}/$ $^{144}\text{Nd})_i$	$\epsilon_{\text{Nd}}(t)$	t_{DM2} (Ma)	$^{206}\text{Pb}/$ ^{204}Pb	$^{207}\text{Pb}/$ ^{204}Pb	$^{208}\text{Pb}/$ ^{204}Pb	$^{238}\text{U}/$ ^{204}Pb	$\Delta\beta$	$\Delta\gamma$
TWG01	129	61.5	658	0.26384	0.70357	13.83	67.34	0.12903	0.5126	0.51221	2.1	893	18.429	15.537	38.204	9.34	13.75	24.92
TWG04	129	72.5	652	0.31428	0.70352	4.93	23.94	0.12943	0.51277	0.51221	5.5	621	18.386	15.523	38.142	9.32	12.87	23.64
TWG05	129	98.8	557	0.50094	0.70299	4.48	23.48	0.11987	0.51281	0.51221	6.6	544	18.389	15.519	38.133	9.31	12.59	23.13
TWG06	129	88.1	776	0.32055	0.70352	4.74	23.28	0.12786	0.51274	0.51221	4.9	671	18.387	15.516	38.143	9.3	12.41	23.59

These samples have relatively low initial $(^{87}\text{Sr}/^{86}\text{Sr})_i$ ratios, ranging from 0.70299 to 0.70357, and initial $(^{143}\text{Nd}/^{144}\text{Nd})_i$ values ranging from 0.51260 to 0.51281, with an average of 0.512363. The $\epsilon_{\text{Nd}}(t)$ values are all positive, ranging from +2.1 to +6.6, and the t_{DM1} (Ma) ranges from 551 Ma to 992 Ma, while the t_{DM2} ranges from 544 Ma to 839 Ma. The Pb isotope data in the study area indicate that the $^{206}\text{Pb}/^{204}\text{Pb}$, $^{207}\text{Pb}/^{204}\text{Pb}$, and $^{208}\text{Pb}/^{204}\text{Pb}$ ratios of the volcanic rocks of the Longjiang formation range from 18.397 to 18.429, 15.516 to 15.54, and 38.189 to 38.2, respectively, and are like the Pb isotopic compositions of the Mesozoic volcanic rocks in the southern Da Hinggan mountains [53].

4.4. Zircon Lu–Hf Isotopes Dating

The results of the zircon Lu–Hf isotope analyses of the volcanic rocks of the Longjiang formation in the Manda Banke area in the central section of the Da Hinggan mountains are listed in Table 4. The $^{176}\text{Lu}/^{177}\text{Hf}$ ratios of the samples in the study area range from 0.0009 to 0.0020, all of which are positive, with an average of 0.0013, which is less than 0.002. This indicates extremely low radiogenic Hf accumulation after zircon formation. Except for one sample (TWG01-5) with a negative $\epsilon_{\text{Hf}}(t)$, the volcanic rocks of the Longjiang formation in the study area have positive $\epsilon_{\text{Hf}}(t)$ values ranging from +1.31 to +43.77, with an average of +8.47. The one-stage Hf model ages (t_{DM1}) range from 538 Ma to 1059 Ma, with an average of 733 Ma, while the two-stage model ages (t_{DM2}) range from 655 Ma to 1427 Ma, with an average of 893 Ma.

Table 4. Zircon Lu–Hf isotope data of Lengjimanda plate of the Longjiang formation volcanic rocks.

Sample	$^{176}\text{Hf}/^{177}\text{Hf}$	2σ	$^{176}\text{Lu}/^{177}\text{Hf}$	1σ	$^{176}\text{Yb}/^{177}\text{Hf}$	1σ	Age (Ma)	$\epsilon_{\text{Hf}}(0)$	$\epsilon_{\text{Hf}}(t)$	$t_{\text{DM1}}(\text{Ma})$	$t_{\text{DM2}}(\text{Ma})$	$f_{\text{Lu/Hf}}$
TWG01-2	0.283935	0.000043	0.003236	0.000004	0.076078	0.000195	126	41.3	43.77	1059	1305	−0.9
TWG01-3	0.282729	0.000039	0.00176	0.000018	0.041094	0.000427	130	−1.4	1.31	751	911	−0.95
TWG01-4	0.282749	0.000049	0.001616	0.000012	0.037553	0.000303	129	−0.7	2.01	719	874	−0.95
TWG01-5	0.282444	0.000034	0.002004	0.000044	0.046304	0.001074	132	−11.5	−8.76	1168	1427	−0.94
TWG01-6	0.282819	0.000045	0.001756	0.000009	0.040134	0.000245	135	1.8	4.6	621	746	−0.95
TWG01-8	0.282862	0.000038	0.001333	0.000012	0.029231	0.000249	130	3.3	6.03	553	668	−0.96
TWG01-10	0.282806	0.000038	0.000989	0.000026	0.021776	0.000614	129	1.3	4.08	627	768	−0.97
TWG01-11	0.282852	0.000041	0.001193	0.000008	0.027001	0.000203	127	2.9	5.63	565	687	−0.96
TWG01-16	0.282868	0.000033	0.000959	0.000016	0.021678	0.000368	130	3.5	6.3	538	655	−0.97

5. Discussion

5.1. The Age of the Longjiang Formation's Volcanic Rocks

Several previous studies have determined to resolve the age of the volcanic rocks in the Longjiang formation. However, as mentioned above, these studies have mainly focused on the northern part of the Great Xing'an mountains. Li [15] used laser fusion $^{40}\text{Ar}/^{39}\text{Ar}$ dating and zircon U–Pb dating to determine that the Longjiang formation in the Longjiang basin, located between the Dayangshu basin in the north and the Lujiaobao depression in the south, is of an Early Cretaceous age of 122 to 126 Ma; Ye [30] obtained an age of 124.63 Ma for the Longjiang formation's volcanic rocks in the Dongpo Xinliuzhan area of the northern section of the Da Hinggan mountains using LA-ICP-MS zircon U–Pb dating; Chen [54] obtained an age of 120.43 Ma for the volcanic rocks of the Longjiang formation in the Shiwuliqiao gold mining area, Heilongjiang province, by performing zircon U–Pb dating on andesite samples. This age belongs to the Early Cretaceous. We obtained relatively accurate ages for the volcanic rocks of the Longjiang formation.

The samples used for dating in the present study are trachyandesite (TWG01, TWG04, and TWG06) and trachyte trachydacite (TWG05). The CL images (Figure 3) show that these zircons have typical zoning structures, and the Th/U ratios range from 0.1989 to 1.7105, indicating that these zircons are of a magmatic origin. The LA-ICP-MS zircon U–Pb weighted mean age of 81 sample points is determined to be 129.0 ± 0.86 Ma (MSWD of 1.06, Figure 7f). This age is consistent with the previous dating results of 120–126 Ma [40] and is within the error range. Based on a thorough analysis of the above studies, it is concluded that the volcanic rocks of the Longjiang formation were formed during the Early Cretaceous.

5.2. The Genesis of the Longjiang Formation's Volcanic Rocks

There are currently several theories of the genesis of calc-alkaline andesites: the mixing of felsic magmas from the crust and mafic magmas from the mantle [55]; the separation and crystallization of mafic magmas from the mantle [56,57]; partial melting of the mantle wedge triggered by subduction fluids or melts [58,59]; and partial melting of lower crustal material triggered by the underplating of mafic magma of a mantle origin [60,61]. Our analysis of the major and trace elements in the samples (Table 1) indicates that the dominant volcanic rocks in the study area are trachyandesite, trachyte trachydacite, and andesite. These volcanic rocks collectively form a suite of intermediate calc-alkaline volcanic rock combinations. The Mg# values (averaging 37.85), Cr content (averaging 12.11 ppm), and Ni contents (averaging 8.80 ppm) of these volcanic rocks are relatively low, much lower than the Mg# values (65–75) of mantle-derived magmas and the Cr and Nd contents (185 ppm and 16 ppm, respectively) of the crust [52,62]. Furthermore, there are no dark mafic enclaves in the volcanic rocks within the study area, indicating that their formation cannot be attributed to the mixing of crustal and mantle-derived magmas [63]. The volcanic rocks in the study area have relatively high K/Rb ratios, with an average of 342 (>110), Zr/Hf ratios with an average of 39 (>30), and Nb/Ta ratios with an average of 15 (>5) [52,64], which indicates that the studied volcanic rocks are not highly fractionated plutonic rocks (Wu et al., 2004; Li et al., 2018). In the La vs. La/Yb plot and La vs. La/Sm plot (Figure 8), the andesite samples show a partial melting trend rather than fractional crystallization,

indicating a weak fractional crystallization process. This suggests that the volcanic rocks in the study area cannot be attributed to mantle-derived magma by means of fractional crystallization [63].

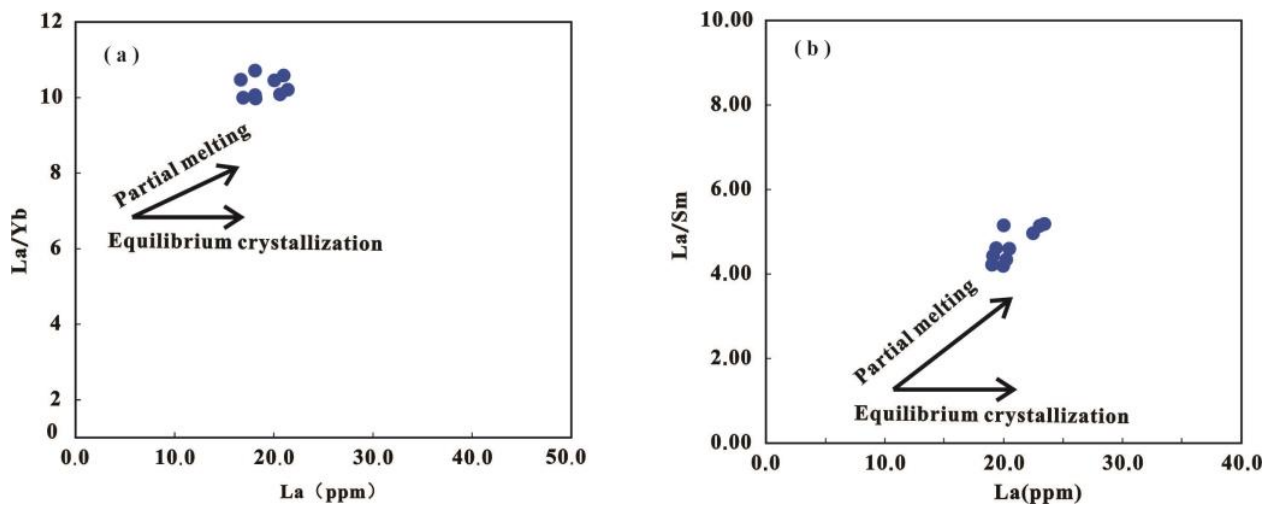


Figure 8. Illustration of magmatic evolution of volcanic rocks in the Longjiang formation of Lengjijimanda plate [65]. (a) La/Yb vs. La and (b) La/Sm vs. La.

The volcanic rocks of the Longjiang formation show relatively high contents of SiO₂ (average 63.17%), Al₂O₃ (average 16.75%), and K₂O (average 3.22%), and low contents of MgO (average 1.87%) and Mg[#] (average 37.85). These characteristics are significantly different from magmas produced by the partial melting of mantle material and are closer to magmas produced by the partial melting of lower crustal material (Mg[#] < 40) [66]. The volcanic rocks of the Longjiang formation in the study area exhibit a moderately negative Eu anomaly, with average Sr/Y and La/Yb ratios of 27.6 and 15.8, respectively. These ratios are not consistent with the characteristics of adakite rocks (>40, >20) [67–69]. In the Sr/Y-Y diagram and the (La/Yb)_N vs. (Yb)_N diagram (Figure 9), all sample compositions fall within the typical island arc rock field. This indicates that the volcanic rocks of the Longjiang formation are predominantly island arc volcanic rocks rather than adakite rocks, and the volcanic rocks in question exhibit characteristics of large ion lithophile element enrichment and high-field-strength element depletion, as seen in the rare earth element distribution pattern and trace element spider diagram (Figure 6). This pattern is similar to that of the lower crust, indicating that the rocks may have originated from the partial melting of basaltic crustal materials. Additionally, the average ratios of Rb/Sr, Ti/Zr, and Ti/Y in the volcanic rock samples from the Longjiang formation in the study area are 0.13, 20.91, and 199.00, respectively. These values are significantly higher than the range of ratios found in mantle-derived magmas (0.03, <20, <100) [52,64,70]. We infer that the primary magma of the volcanic rocks in the Lengjijimanda plate of the Longjiang formation originated from the partial melting of basaltic crustal materials rather than the mantle.

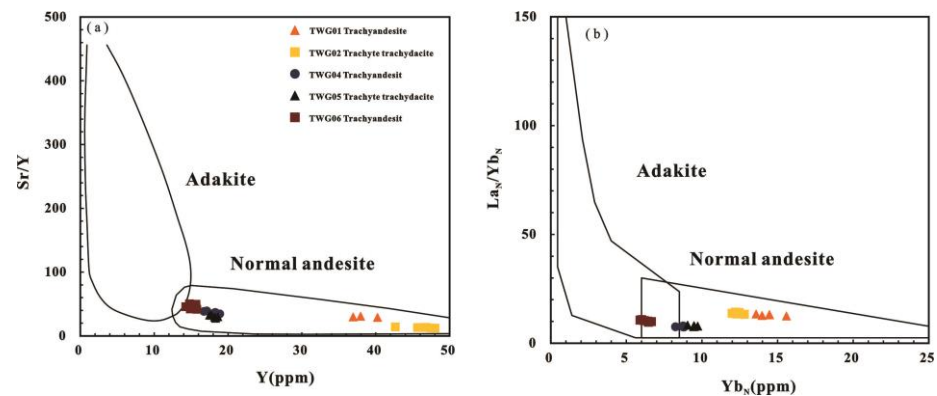


Figure 9. Adakite discrimination diagram of Longjiang formation volcanic rocks, Lengjimanda plate. (a) Sr/Y vs. Y diagram; (b) $(La/Yb)_N$ vs. $(Yb)_n$ diagram [71].

Zircon Hf isotope studies conducted in the Lengjimanda plate indicate positive $\epsilon_{Hf}(t)$ values ranging from +1.31 to +43.77, with an average of +8.47, except for one sample with negative values; the two-stage Hf model ages (t_{DM2}) range from 655 to 1427 Ma. The $\epsilon_{Hf}(t)$ values are relatively uniform and high, indicating that the rocks are derived directly from the mantle or from basaltic crust formed by the melting of depleted mantle. The presence of a negative $\epsilon_{Hf}(t)$ value of -8.76 suggests the possible involvement of ancient crust in the rock formation process. In the $\epsilon_{Hf}(t)$ vs. age diagram (Figure 10), all the samples' compositions fall within the range of granulite meteorites and depleted mantle, which suggests that the magma may have originated from the partial melting of basaltic crustal materials that were newly generated from the depleted mantle during the Neoproterozoic to Phanerozoic period [35,72,73]. This hypothesis is consistent with the large-scale crustal accretion event that occurred in the Da Hinggan mountain region during the Neoproterozoic to Phanerozoic period, as reported by Sui [74] and Wang [75]. The Longjiang formation's volcanic rocks in the study area exhibit higher average ratios of Nb/Ta and Zr/Hf, 14.51 and 39.39, respectively, compared to the average values in the crust (13.00, 33.00) [64,76]; these values are similar to the average values in the mantle (17.50, 37.00) [52]. According to Shi [77], the magma source area is composed of recently generated crustal materials from the depleted mantle.

The study area's volcanic rock samples display $^{87}Sr/^{86}Sr$ ratios ranging from 0.703 to 0.7036, all of which are below 0.705. The $\epsilon_{Nd}(t)$ values range from +2.1 to +6.6, and the $\epsilon_{Sr}(t)$ values range from -10.7 to -19.2 . In Figure 11's $\epsilon_{Nd}(t)$ vs. $\epsilon_{Sr}(t)$ diagram, all the volcanic rock sample compositions from the Longjiang formation in the study area fall within quadrant II, which indicates that the magma source of the volcanic rocks in the area is related to the depleted mantle, as noted by Hou [78] and Shao [79]. The Pb isotope data from the study area indicate that the volcanic rocks of the Longjiang formation exhibit uranium lead enrichment and thorium lead depletion. The $^{207}Pb/^{204}Pb$ ratios range from 15,516 to 15,540, which are greater than 15,530; the $^{208}Pb/^{204}Pb$ ratios range from 38,189 to 38,200, which are lower than 39,000; and the $^{206}Pb/^{204}Pb$ ratios range from 18,397 to 18,429, which are greater than 18,000. In the genetic classification diagram of $\Delta\gamma$ vs. $\Delta\beta$ (Figure 12a) by Zhu [80] and in the tectonic model diagrams of $^{206}Pb/^{204}Pb$ vs. $^{207}Pb/^{204}Pb$ and $^{206}Pb/^{204}Pb$ vs. $^{208}Pb/^{204}Pb$ (Figure 12b–d), the samples are distributed in the lead region of the subduction zone, where the crust and mantle mix; this suggests that the magma may have originated from the partial melting of basaltic crustal materials that were newly generated from the depleted mantle. This is consistent with the findings of Tan [70], Gao [81], and Jia [82] regarding the petrogenesis of Early Cretaceous volcanic rocks in the Soren and Handagai areas of the central Da Hinggan mountains.

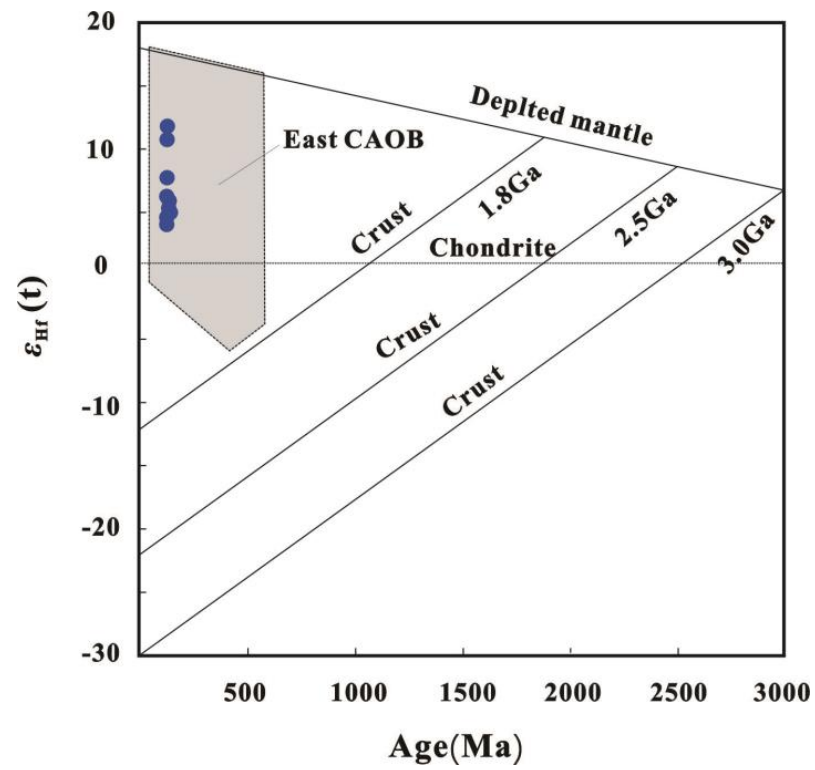


Figure 10. $\epsilon_{Hf}(t)$ vs. age diagram of Longjiang formation volcanic rocks, Lengjimanda plate. East CAOB: East Asian Orogenic Belt Eastern part [21].

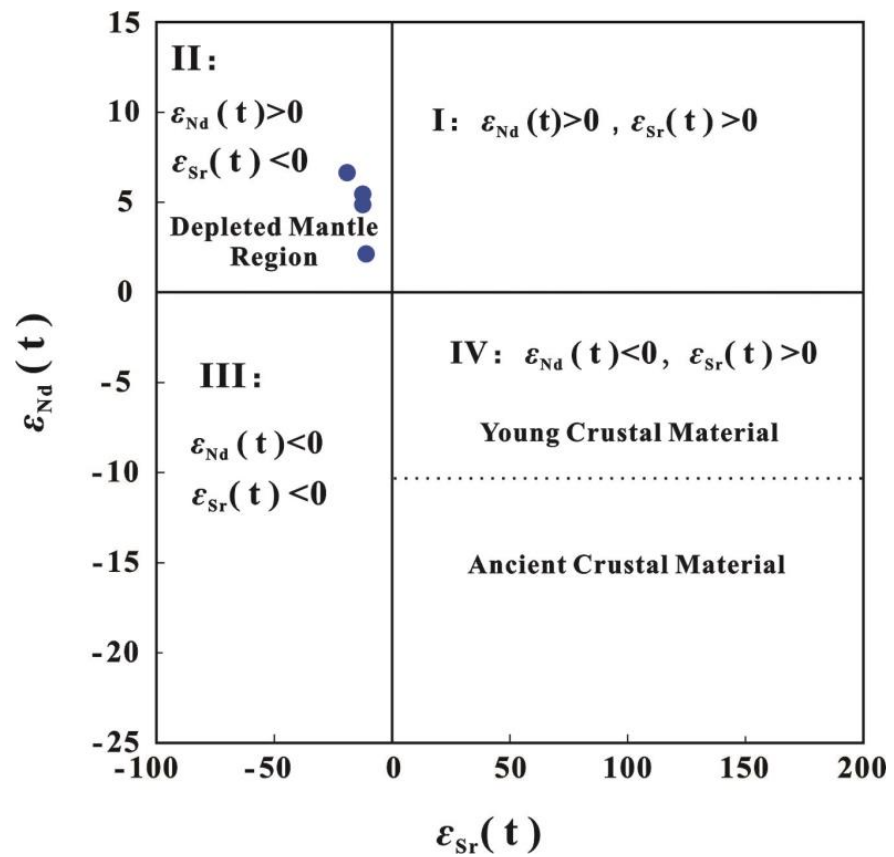


Figure 11. $\epsilon_{Nd}(t)$ vs. $\epsilon_{Sr}(t)$ diagram of volcanic rocks in the Longjiang formation of Lengjimanda plate.

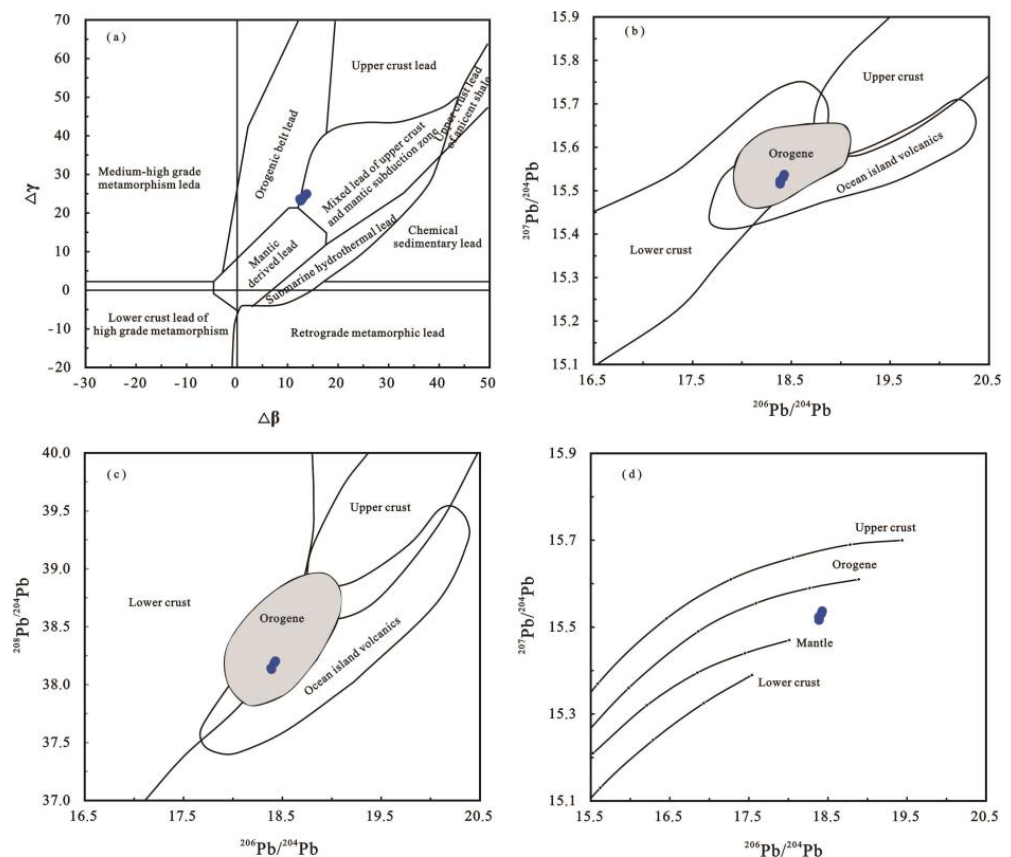


Figure 12. Pb isotope composition diagram of Longjiang formation volcanic rocks, Lengjimanda plate. Orogene: Orogenic belt. ((a), [83]; (b,c), [84]; (d), [80]).

Based on the geochemical characteristics and zircon Hf analyses, as well as the whole-rock Sr–Nd–Pb isotopes, we conclude that the volcanic rocks of the Longjiang formation in the Lengjimanda plate region were generated through the partial melting of the lower crust, and the magma’s source material is believed to be basaltic crustal material that was newly generated from the depleted mantle.

5.3. Tectonic Background

There are different theories regarding the tectonic environment that was responsible for the formation of the Mesozoic volcanic rocks in the Da Hinggan mountain region. They include the subduction of the ancient Pacific plate [20,85], a mantle plume origin [12,86], and the subduction of the Mongol–Okhotsk Ocean [11,87]. However, closure of the Mongol–Okhotsk Ocean and subduction of the Pacific plate have been identified as the combined cause in various studies [18,88–92].

Previous data suggest that during the Mesozoic era, the Da Hinggan mountain region underwent the superposition and reformation of the ancient Pacific plate and the Mongolian–Okhotsk plate [88,92]. Early studies indicate that the Mongolian–Okhotsk Ocean closed during the Middle Late Jurassic period [93] and had little influence on the late Mesozoic magmatic activity in the Da Hinggan mountain region. Recently, researchers provided evidence for the existence of a southward subduction of the Mongolian–Okhotsk plate during the Mesozoic era; for instance, Badarch [94] divided the tectonic blocks and established a new stratigraphic column. Discovering the presence of Permo–Triassic accretionary terranes in the Mongolian–Okhotsk suture zone, Chen [95] identified Late Triassic Inner Mongolia Taipingchuan porphyry copper–molybdenum deposits. Zeng [59] obtained geochemical data and concluded that the Badaguan metamorphic complex in the Erguna area was formed due to the subduction of the Mongolian–Okhotsk Ocean towards

the Erguna block. These studies provide evidence for the southward subduction of the Mongolian-Okhotsk plate during the Mesozoic era, and many researchers believe that the Late Mesozoic magmatic activity in the Da Hinggan mountain area is related to the extensional environment after the closure of the Mongol-Okhotsk Ocean. This view is supported by Meng [87], Ying [96], Sun [97], Li [98], and Si [99]. Additionally, numerous scholars posit that the Mesozoic volcanic rocks in the Da Hinggan mountains region are closely linked to the subduction of the ancient Pacific plate. Kong conducted a study on the tectonic background of the volcanic rocks in the Khorchin area and concluded that they were primarily influenced by the subduction of the ancient Pacific plate. Tang [41] summarized the petrological composition and geochemical characteristics of Mesozoic Cenozoic volcanic rocks in the Northeast Asian margin and suggested that the ancient Pacific plate underwent low-angle subduction towards Northeast Asia in the Early Cretaceous. Yang [100] conducted research on the paleontology, regional comparisons, and chronology in the Da Hinggan mountain area and concluded that the Early Cretaceous volcanic rocks (145–110 Ma) in the Da Hinggan mountain region are generally distributed in an NNE direction, which is consistent with the mechanism of subduction of the ancient Pacific plate.

During the late Early Cretaceous period, volcanic rocks were widely distributed across the Da Hinggan mountain area, which exhibited a typical bimodal volcanic rock assemblage [101]. The region also showed an extensional environment at the regional scale [92,100,102]. The volcanic activity in the Da Hinggan mountain area during this period was influenced by the closure of the Mongol-Okhotsk suture zone [7,103] and the subduction of the ancient Pacific plate beneath the Eurasian continent [9,104,105]. Our study area's volcanic rocks consist mainly of a suite of Early Cretaceous (129.00 ± 0.78 Ma) intermediate volcanic rocks. These rocks have a high SiO₂ content and are enriched in large-ion lithophile elements while being depleted in high-field-strength elements. Furthermore, there is an obvious fractionation of light and heavy rare earth elements. In the microelement tectonic environment discrimination diagram of the Longjiang formation's volcanic rocks in the study area (Figure 13), they mainly exhibit characteristics of a post-collisional environment, while some samples also show features of a continental arc environment. This indicates that the Early Cretaceous volcanic rocks in the Longjiang formation were formed in a superimposed environment of post-collision and continental arc. Combined with a regional background analysis, it is believed that the tectonic setting in the study area may be related to the closure of the Mongol-Okhotsk Ocean and the oblique subduction of the ancient Pacific plate. This view is supported by Zhang [17], Zhang [36], Zhang [106], and Xu [7], who suggested that the Da Hinggan mountain area was affected by the closure of the Mongol-Okhotsk Ocean and the oblique subduction of the ancient Pacific plate during the Early Cretaceous.

The tectonic background of the volcanic rocks formed in the Longjimanda plate of the Heilongjiang Group reflects the alternating influence of the Mongol-Okhotsk oceanic plate and the ancient Pacific plate on the Mesozoic volcanic rocks of the Da Hinggan mountains. A synthesis of previous research indicates that the Mesozoic volcanic rocks in the Greater Khingan Range were primarily influenced by the closure of the Mongol-Okhotsk Ocean during the Late Jurassic to Early Cretaceous period. During the Early Cretaceous period, the region may have been affected by the closure of the Mongol-Okhotsk Ocean and the subduction of the ancient Pacific plate. Subsequently, during the Early Cretaceous, they were primarily influenced by the subduction of the ancient Pacific plate.

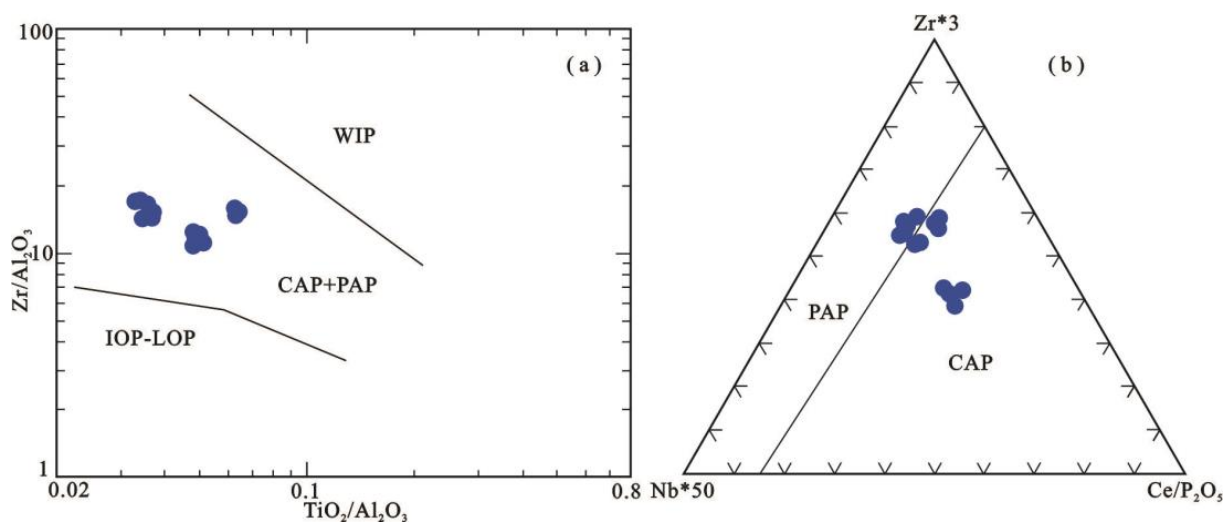


Figure 13. Structural identification diagram of volcanic rocks in Longjiang formation, Lengjimanda plate [107]. (a) Intraplate environment (WIP), (b) continental arc environment (CAP), post-collision environment (PAP), initial ocean arc environment (IOP), late ocean arc environment (LOP).

6. Conclusions

The volcanic rocks of the Longjiang formation in the Lengjimanda plate in the middle section of the Da Hinggan mountains are predominantly intermediate basic volcanic rocks, comprising porphyritic rock, porphyritic andesite, and andesite. The LA-ICP-MS zircon U–Pb analysis suggested an age of 129.0 ± 0.86 Ma (MSWD = 1.06, $n = 81$), which suggests that these rocks were formed during the Early Cretaceous period. Petrological, geochemical, and isotopic studies of the Longjiang formation’s volcanic rocks indicate that they are the result of the partial melting of the lower crust. The source material for these rocks is newly generated basaltic crustal material from a depleted mantle. These rocks are believed to have formed in a setting of post-collision and continental arc superposition. Their tectonic background may be related to the closure of the Mongolian-Okhotsk Ocean and the oblique subduction of the ancient Pacific plate, as indicated by the regional tectonic evolution history.

This study posits that the regional volcanic eruption event that occurred approximately 130 million years ago in the Lengjimanda plate coincided with the transitional period of the Da Hinggan mountains from rapid uplift to slow uplift, as well as the period of oblique subduction of the ancient Pacific plate beneath East Asia. This finding has significant implications for the analysis of the Early Cretaceous basin’s evolution and stratigraphic subdivision in this region. The research on the tectonic background of the Lengjimanda plate presented in this paper demonstrates the alternating influence of the Mesozoic Mongol-Okhotsk oceanic plate and the ancient Pacific plate on the timing of the Da Hinggan mountain region. The Mesozoic volcanic rocks in the Da Hinggan mountains were significantly influenced by the closure of the Mongol-Okhotsk Ocean during the Late Jurassic to Early Cretaceous period. During the Early Cretaceous period, these rocks may have been affected by two distinct geological processes: the closure of the Mongol-Okhotsk Ocean and the subduction of the ancient Pacific plate. Subsequently, during the early Early Cretaceous, they were primarily influenced by the subduction of the ancient Pacific Ocean. This information is useful in delineating the periods in which the Mongol-Okhotsk oceanic plate and the ancient Pacific plate influenced the Da Hinggan mountains.

This article presents a petrological, zircon U–Pb geochronological, geochemical, and isotope chemical analysis of the volcanic rocks in the Longjiang formation, thereby determining the formation age of these rocks in the region. The article discusses the origin and tectonic background of the volcanic rocks, reconstructs the regional geodynamic evolution, fills the research gap concerning the Longjiang volcanic rocks, and provides reliable data

on the dynamic history of the Da Hinggan mountain region. Moreover, the study provides avenues for further geological exploration and geophysical detection in the region.

Supplementary Materials: The following supporting information can be downloaded at: <https://www.mdpi.com/article/10.3390/min14070719/s1>, Table S1: Zircon LA-ICP-MS U-Pb data of the volcanic rocks from Lengjimanda plate of the Longjiang formation. Table S2: Major and trace element compositions of Lengjimanda plate of the Longjiang formation volcanic rocks. Table S3: Sr-Nd-Pb isotopic data of the Longjiang Formation volcanic rocks. Table S4: Zircon Lu-Hf isotope data of Lengjimanda plate of the Longjiang Formation volcanic rocks.

Author Contributions: Methodology, S.Z.; investigation, Z.T.; data curation, L.S.; writing—original draft preparation, S.-C.W.; writing—review and editing, Y.-J.H. All authors have read and agreed to the published version of the manuscript.

Funding: This research received no external funding.

Data Availability Statement: The authors confirm that the data supporting the findings of this study are available within the article and its Supplementary Materials.

Acknowledgments: Thank you very much to all the teachers for their contributions during the paper writing process. Teacher Yu Jie Hao provided review and annotation guidance throughout the writing of the paper. Teacher Lu Shi provided significant assistance with data processing for the article. Teacher Zhen Tang provided much help during field geological surveys. Teacher Shuang Zhu provided valuable assistance with paper revisions and writing techniques. This work was supported by the geological survey project of China “Regional Geological Survey of Ergun Area, Inner Mongolia 1:50,000 geological map including Lengjimanda Plate, Jirigen Linchang, Ximalatu, Wulanzhao, Bayantao Sea” (DD20160048-02).

Conflicts of Interest: The authors declare no conflict of interest.

References

1. Wu, F.Y.; Sun, D.Y.; Lin, Q. Genesis and crustal accretion of the Epigenetic granites in Northeast China. *J. Petrol.* **1999**, 22–30.
2. Hong, D.W.; Wang, S.K.; Xie, X.L.; Zhang, J.S.; Wang, T. Relationship between supercontinental evolution and continental crustal growth from positive $\epsilon(\text{Nd})$ -valued granites in Central Asia. *J. Geol.* **2003**, 203–209.
3. Kuzmin, M.L.; Abramovich, G.Y.A.; Dril, S.L.; Kravchinsky, V.Y.A. The Mongolian-Okhotsk suture as the evidence of Late Paleozoic-Mesozoic collisional processes in Central Asia. In Proceedings of the 30th IGC, Beijing, China, 4–14 August 1996; pp. 1–261.
4. Zhao, X.X.; Coe, R.S. Paleomagnetic constraints on the paleogeography of China: Implications for Gondwanaland. In Proceedings of the 30th IGC, Beijing, China, 4–14 August 1996; pp. 1–231.
5. Zhao, Z. Late Paleozoic Magmatism and Its Tectonic Significance in Northern Daxinganling. Ph.D. Thesis, Jilin University, Changchun, China, 2011.
6. Sengor, A.; Natal'in, B. Paleotectonics of Asia: Fragments of a synthesis. *Tecton. Evol. Asia* **1996**, 1–129.
7. Xu, W.L.; Wang, F.; Pei, F.P.; Meng, E.; Tang, J.; Xu, M.J.; Wang, W. Mesozoic tectonic regime and regional mineralization context in northeast China: Constraints from temporal and spatial variations of Mesozoic volcanic assemblages. *J. Petrol.* **2013**, 30, 339–353.
8. Xu, W.L.; Ji, W.Q.; Pei, F.P.; Meng, E.; Yu, Y.; Yang, D.B.; Zhang, X.Z. Triassic volcanism in eastern Heilongjiang and Jilin provinces, NE China: Chronology, geochemistry, and tectonic implications. *J. Asian Earth Sci.* **2009**, 34, 392–402. [[CrossRef](#)]
9. Wu, F.Y.; Sun, D.Y.; Ge, W.C.; Zhang, Y.B.; Grant, M.L.; Wilde, S.A.; Jahn, B.M. Geochronology of the Phanerozoic granitoids in northeastern China. *J. Asian Earth Sci.* **2011**, 41, 1–30. [[CrossRef](#)]
10. Li, S.T.; Yang, S.K.; Wu, C.L.; Huang, J.F.; Cheng, S.T.; Xia, W.C.; Zhao, G.Y. Late Mesozoic rifting in northeastern China and the Northeast Asian fault basin system. *Chin. Sci. (Ser. B) Chem. Biol. Agron. Med. Geol.* **1987**, 185–195.
11. Lin, Q.; Ge, W.C.; Cao, L.; Sun, D.Y.; Lin, J.K. Geochemical characterization of Mesozoic bimodal volcanic rocks in the Daxinganling. *Geochemistry* **2003**, 208–222.
12. Ge, W.C.; Lin, Q.; Sun, D.Y.; Wu, F.W.; Won, J.-K.; Lee, W.Y.; Chen, M.S.; Yoon, S.-H. Geochemical characterization of Mesozoic basalts in Daxing'anling: Evidence for crust-mantle interaction. *J. Petrol.* **1999**, 396–406.
13. Ge, W.C.; Wu, F.Y.; Zhou, C.Y.; Zhang, J.H. Zircon U-Pb ages and geologic significance of Mesozoic granites from the Wulanhote area, central Daxinganling. *J. Petrol.* **2005**, 21, 14.
14. Zhang, L.C.; Chen, Z.G.; Zhou, X.H.; Ying, K.F.; Wang, F.; Zhang, Y.T. Deep source zones and tectono-magmatic evolution of Early Cretaceous volcanic rocks in the Genhe area, Daxing'anling: Sr-Nd-Pb-Hf isotope geochemical constraints. *J. Petrol.* **2007**, 61, 1594–1612.
15. Li, Y.F.; Bian, X.F.; Gao, X.Y.; Chen, S.W.; Ding, Q.H. Laser total-melt $^{40}\text{Ar}/^{39}\text{Ar}$ dating of Mesozoic volcanic rocks in the Longjiang Basin, northern Daxinganling. *Geol. Bull.* **2013**, 32, 1212–1223.

16. Zhang, P.C.; Peng, B.; Zhao, J.Z.; Zhang, Z.F.; Zhao, J.; Guo, G.F. Zircon U-Pb chronology, geochemistry and metallogenic significance of the Hai Liyu extraordinarily high-divergence granitoids from the southern Daxinganling section. *J. Rock Mineral.* **2022**, *41*, 1029–1046.
17. Sui, Z.M.; Ge, W.C.; Xu, X.C.; Zhang, J.H. Characteristics of the Late Paleozoic post orogenic granitoids from Station XII, Daxinganling and their geological significance. *J. Petrol.* **2006**, *2679–2686*.
18. Chen, Z.G.; Zhang, L.C.; Zhou, X.C.; Wan, B.; Ying, K.F.; Wang, F. Chronological and geochemical characterization of volcanic rock sections from Xinyuqi, Manzhouli. *J. Petrol.* **2006**, *22*, 2971–2986.
19. Zhang, Y.B.; Sun, S.H.; Honma, H.J.; Mao, Q. Mixing of Mesozoic acidic magmas in the Linxi area, southern Daxinganling. *J. Petrol.* **2003**, *19*, 16.
20. Zhang, J.H. Chronology and Geochemistry of Mesozoic Volcanic Rocks in Daxing'anling. Ph.D. Thesis, China University of Geosciences, Wuhan, China, 2009.
21. Yang, B.H.; Wang, W.D.; Yan, Y.S.; Wei, X.Y.; Ge, C.B. Genesis and mantle enrichment of volcanic rocks in the Tamulangou formation, Xinlin District, northern Daxinganling. *Geol. Rev.* **2016**, *62*, 16.
22. Ji, Z.; Ge, W.C.; Yang, H.; Zhao, G.C.; Wang, Q.H.; Bi, J.H. Chronology and geochemistry of volcanic rocks from the Manketou Ebo formation, middle Daxinganling. In *Abstracts from the 15th Annual Academic Conference of the Geological Association of China, Mineral and Rock Geochemistry Division (Volume 1)*; The Geological Association of Canada: St. John's, NL, Canada, 2015.
23. Shang, Y.H.; Lu, S. Chronology, geochemical characteristics and petrogenesis of the Manitu formation, Daxing'anling. *Heilongjiang Univ. Sci. Technol.* **2017**, *27*, 6.
24. Zhang, L.Q.; Chen, B.; Cao, Y.B.; Wang, J.H.; Huang, Z.J.; Chen, G.Y. Chronology and petrogeochemical characterization of the volcanic rocks of the Manitu formation, Horqin Youyiqian Banner, Inner Mongolia. *Mod. Min.* **2017**, *33*, 5.
25. Zhang, L.T.; Li, S.C.; Zhao, Q.Y.; Li, X.F.; Wang, L.; Li, Z.H. Age of formation and geochemical characteristics of volcanic rocks of the Baiyin Gao Lao formation, middle Daxinganling. *World Geol.* **2015**, *44–54*.
26. Nie, L.J.; Jia, H.M.; Wang, C.; Lu, X.B. Chronology, geochemistry and its geological significance of rhyolite from the Baiyin Gao Lao formation, middle Daxinganling. *World Geol.* **2015**, *34*, 296–304.
27. Ding, Q.H.; Chen, S.W.; Shang, L.; Li, Y.F.; Wang, J. New understanding of the Lower Cretaceous Longjiang formation in eastern Daxinganling. *Geol. Resour.* **2014**, *23*, 8.
28. Zhang, C.; Wu, X.W.; Zhang, Y.J.; Guo, W.; Quan, J.Y. LA-ICP-MS zircon U-Pb ages of alkali flowstone from Guanghua formation, Longjiang Basin, northern Daxinganling and their geological significance. *Geol. Bull.* **2017**, *36*, 11.
29. Li, Y.F.; Gao, X.Y.; Bian, X.F.; Chen, S.W.; Ding, Q.H. LA-ICP-MS zircon U-Pb ages, geochemical characteristics and their geological significance of Mesozoic volcanic rocks in the Longjiang Basin, northern Daxinganling. *Geol. Bull.* **2013**, *1195–1211*.
30. Ye, S.P.; Wei, J.; Sha, X.B. Characteristics and tectonic environment of volcanic rocks of the Longjiang formation in the Xinliu Station area, Daxing'anling. *World Nonferrous Met.* **2017**, *200+202*.
31. Amelin, Y.; Lee, D.C.; Halliday, A.N.; Pidgeon, R.T. Nature of the earth's earliest crust from hafnium isotopes in single detrital zircons. *Nature* **1999**, *399*, 1497–1503. [[CrossRef](#)]
32. Amelin, Y.; Lee, D.C.; Halliday, A.N. Early-middle archaean crustal evolution deduced from lu-hf and u-pb isotopic studies of single zircon grains. *Geochim. Cosmochim. Acta* **2000**, *64*, 4205–4225. [[CrossRef](#)]
33. Griffin, W.L.; Belousova, E.; Se, J.; Sy VA, E.O.; Sr, S.; Nj, P. The hf isotope composition of cratonic mantle: LAM-MC-ICPMS analysis of zircon megacrysts in kimberlites. *Geochim. Cosmochim. Acta J. Geochem. Soc. Meteorit. Soc.* **2000**, *64*, 133–147. [[CrossRef](#)]
34. Wiedenbeck, M. Three natural zircon standards for U-Th-Pb, Lu-Hf, trace element and ree analyses. *Geostand. Newsl.* **1995**, *19*, 1–23. [[CrossRef](#)]
35. Wu, F.Y.; Li, X.H.; Zheng, Y.F.; Gao, G. Lu-Hf isotope system and its petrological applications. *J. Petrol.* **2007**, *23*, 36.
36. Zhang, Y.T.; Zhang, L.C.; Ying, K.F.; Zhou, X.H.; Wang, F.; Hou, Q.L. Geochemical and source-area characterization of Early Cretaceous volcanic rocks in the Tahe area, northern Daxinganling. *J. Petrol.* **2007**, *23*, 2811–2822.
37. Zhang, J.H.; Ge, W.C.; Wu, F.Y.; Wilde, S.A.; Yang, J.H.; Liu, X.M. Large-scale Early Cretaceous volcanic events in the northern Great Xing'an Range, Northeastern China. *Lithos* **2008**, *102*, 138–157. [[CrossRef](#)]
38. Li, J.Y. New understanding of some geotectonic problems in northeast China and neighboring areas. *Geol. Rev.* **1998**, *339–347*.
39. Li, J.Y.; Qu, J.F.; Zhang, J. New progress in the study of orogenic process and metallogenic geological background of Tianshan-Xingmeng orogenic mountains. *Geol. Bull.* **2013**, *207–219*.
40. Wu, T. Geochemical Characterization and Tectonic Context of Early Cretaceous Neutral Volcanic Rocks from the Zalantun Area, Inner Mongolia. Master's Thesis, Jilin University, Changchun, China, 2018.
41. Tang, J.; Xu, W.L.; Wang, F.; Ge, W.C. Subduction history of the Paleo-Pacific plate under Eurasia: Mesozoic-Paleocene magma record from the Northeast Asian land margin. *Sci. China Earth Sci.* **2018**, *48*, 35.
42. Zhuo, S.; Ji, A. X-ray fluorescence spectroscopy analysis. *Anal. Lab.* **2003**, *102–108*.
43. Yuan, H.L.; Gao, S.; Liu, X.M.; Li, H.M.; Günther, D.; Wu, F.Y. Accurate U-Pb age and trace element determinations of zircon by laser ablation-inductively coupled plasma-mass spectrometry. *Geostand. Geoanalytical Res.* **2004**, *28*, 353–370. [[CrossRef](#)]
44. Andersen, T. Correction of common lead in U-Pb analyses that do not report ²⁰⁴Pb. *Chem. Geol.* **2002**, *192*, 59–79. [[CrossRef](#)]
45. Sláma, J.; Košler, J.; Condon, D.J.; Crowley, J.L.; Gerdes, A.; Hanchar, J.M.; Horstwood, M.S.; Morris, G.A.; Nasdala, L.; Norberg, N. Plešovice zircon—A new natural reference material for U–Pb and Hf isotopic microanalysis. *Chem. Geol.* **2008**, *249*, 1–35. [[CrossRef](#)]

46. Wei, P.; Gao, J.F.; Zhao, K.D.; Ling, H.F.; Jiang, S.C. Rapid and effective separation of Rb-Sr and Sm-Nd using DCTA and HIBA. *J. Nanjing Univ.* **2005**, *44*, 445–450.
47. Goolaerts, A.; Mettelli, N.; Dejong, J. Hf and Lu isotopic reference values for the zircon standard 91500 by MC-ICP-MS. *Chem. Geol.* **2004**, *206*, 1–9. [[CrossRef](#)]
48. Wu, F.Y.; Lin, J.Q.; Wilde, S.A.; Zhang, X.O.; Yang, J.H. Nature and significance of the Early Cretaceous giant igneous event in eastern China. *Earth Planet. Sci. Lett.* **2005**, *233*, 103–119. [[CrossRef](#)]
49. Irvine, T.N.; Baragar, W.R.A. A Guide to the Chemical Classification of the Common Volcanic Rocks. *Can. J. Earth Sci.* **1971**, *8*, 523–548. [[CrossRef](#)]
50. Maniar, P.D.; Piccoli, P.M. Tectonic discrimination of granitoids. *Geol. Soc. Am. Bull.* **1989**, *101*, 635–643. [[CrossRef](#)]
51. Sun, S.S.; McDonough, W.F. Chemical and isotopic systematics of oceanic basalts: Implications for mantle composition and processes. In *Magmatism in the Ocean Basins*. Geological Society; Sanders, A.D., Norry, M.J., Eds.; Special Publications: London, UK, 1989; Volume 42, pp. 313–345.
52. McDonough, W.F.; Sun, S.S. The composition of the Earth. *Chem. Geol.* **1995**, *120*, 223–253. [[CrossRef](#)]
53. Wu, H.Y.; Zhang, L.C.; Zhou, X.H.; Chen, C.G. Chronological and geochemical characterization and genesis of Late Mesozoic andesites from the middle Daxinganling. *J. Petrol.* **2008**, *24*, 1339–1352.
54. Chen, Z.; Li, X.W.; Zhang, S.J.; Zhou, C.F.; Li, Y.F.; Guo, L. Geochemical characterization and tectonic background analysis of volcanic rocks in the Longjiang formation, Shiwuliqiao Gold Mine, Heilongjiang. *Geol. Resour.* **2019**, 413–422.
55. Kawabata, H.; Shuto, K. Magma mixing recorded in intermediate rocks associated with high-Mg andesites from the setouchi volcanic belt, Japan: Implications for archaic tfg formation. *Volcanol. Geotherm. Res.* **2005**, *140*, 241–271. [[CrossRef](#)]
56. Streck, M.J.; Leeman, W.P.; Chesley, J.T. High-magnesian andesite from mount shasta: A product of magma mixing and contamination, not a primitive melt: Comment and reply. *Geology* **2007**, *35*, e147. [[CrossRef](#)]
57. Qian, Q.; Hermann, R. formation of high-mg diorites through assimilation of peridotite by monzodiorite magma at crustal depths. *J. Petrol.* **2011**, *51*. [[CrossRef](#)]
58. Hanyu, T.; Tatsumi, Y.; Nakai, S.; Chang, Q.; Miyazaki, T.; Sato, K.; Tani, K.; Shibata, T.; Yoshida, T. Contribution of slab melting and slab dehydration to magmatism in the Japanese arc. *Geochim. Cosmochim. Acta* **2006**, *70*, A229. [[CrossRef](#)]
59. Zeng, W.S.; Zhou, J.B.; Dong, C.; Cao, J.L.; Wang, B. A record of Mongolia-Okhotsk ocean subduction: Evidence from the Badaiguan metamorphic mafic rocks in the Erguna region. *J. Petrol.* **2014**, *30*, 1948–1960.
60. Jung, S.; Hoernes, S.; Mezger, K. Synorogenic melting of mafic lower crust: Constraints from geochronology, petrology and Sr, Nd, Pb and O isotope geochemistry of quartz diorites (Damara orogen, Namibia). *Contrib. Mineral. Petrol.* **2002**, *143*, 551–566. [[CrossRef](#)]
61. Ji, Z.; Ge, W.C.; Yang, H.; Bi, J.H.; Yu, Q.; Dong, Y. Late Triassic Andean-type andesites in the middle Daxinganling: A product of southward subduction of the Mongolia-Okhotsk Oceanic Plate. *J. Petrol.* **2018**, *34*, 14.
62. Jung, S.; Masberg, P. Major- and trace-element systematics and isotope geochemistry of Cenozoic mafic volcanic rocks from the Vogelsberg (central Germany): Constraints on the origin of continental alkaline and tholeiitic basalts and their mantle sources. *J. Volcanol. Geotherm. Res.* **1998**, *86*, 151–177. [[CrossRef](#)]
63. Wei, B.Y.; Wu, M.H.; Liu, B.; Jiang, J.B.; Liang, W. Chronology, geochemical characterization and tectonic significance of andesites in the Yamansu area, Eastern Tien Shan. *South. Met.* **2020**, *50*, 14–32.
64. Taylor, S.R.; McLennan, S.M. *The Continental Crust: Its Composition and Evolution*; Blackwell Scientific Publication: Oxford, UK, 1985; pp. 1–132.
65. Keppler, H. Constraints from partitioning experiments on the composition of subduction-zone fluids. *Nature* **1996**, *380*, 237–240. [[CrossRef](#)]
66. Li, C.D.; Zhang, F.Q.; Miao, L.C.; Jie, H.Q.; Xu, Y.W. Late Permian high-magnesium andesite shrimp zircon chronology and geochemical characterization of the Seruohe Late Permian in Jilin. *J. Petrol.* **2007**, *23*, 767–776.
67. Defant, M.J.; Drummond, M.S. Derivation of Some Modern Arc Magmas by Melting of Young Subducted Lithosphere. *Nature* **1990**, *347*, 662–665. [[CrossRef](#)]
68. Zhu, D.C.; Duan, L.P.; Liao, Z.L.; Pan, G.T. Differentiation of two types of adakites. *Mineral. Rocks* **2002**, *22*, 5.
69. Zhang, Q.; Wang, Y.; Wang, Y.L. Edakite and the tectonic environment. *Geotecton. Mineral.* **2003**, *27*, 101–108.
70. Li, C.N. *Trace Element Petrology of Igneous Rocks*; China University of Geosciences Press: Qinhuaungdao, China, 1992.
71. Drummond, M.S.; Bordelon, M.; de Boer, J.Z.; Defant, M.J.; Bellon, H.; Feigenson, M.D. Igneous petrogenesis and tectonic setting of plutonic and volcanic rocks of the Cordillera de Talamanca, Costa Rica-Panama, Central American arc. *Am. J. Sci.* **1995**, *295*, 875–919. [[CrossRef](#)]
72. Tan, H.Y.; He, Z.H.; Chen, F.; Du, Y.D.; Ren, Z.H. Zircon U-Pb ages, geochemical characteristics and tectonic significance of volcanic rocks from the Baiyin Gao Lao formation, Solun area, middle Daxinganling. *Geol. Bull.* **2017**, *36*, 893–908.
73. Hao, Y.J.; Ren, Y.S.; Shi, Y.F.; Shang, Q.Q.; Sun, Z.M.; Gao, Y.; Yang, Q. Age of formation, petrogenesis and tectonic background of the granite porphyry of the porphyry-type tin polymetallic deposits in Hekou Forest, Wundashan District, Heilongjiang Province. *J. Petrol.* **2020**, 837–855.
74. Sui, Z.M.; Ge, W.C.; Wu, F.Y.; Zhang, J.H.; Xu, X.C.; Cheng, R.Y. Zircon U-Pb ages, geochemical characteristics and genesis of Jurassic granitic rocks from northeastern Daxinganling. *J. Petrol.* **2007**, *23*, 20.

75. Wang, Y.L.; Ao, G.; Wang, H.P.; Wang, Z.J.; Wang, Q.; Zhong, M.S. Zircon U-Pb chronology, geochemistry and tectonic significance of Early Cretaceous granitoids from the Solun area, middle Daxinganling. *Geosci. Technol. News* **2019**, *13*.
76. Barth, M.G.; McDonough, W.F.; Rudnick, R.L. Tracking the budget of Nb and Ta in the continental crust. *Chem. Geol.* **2000**, *165*, 197–213. [[CrossRef](#)]
77. Shi, L.; Tang, Z.; Zheng, C.Q.; Qin, T.; Zhang, L.D.; Wang, Y. Petrogenesis and tectonic context of Early Cretaceous neutral volcanic rocks in the Chaihe-Mushroom gas region, central Daxinganling. *Geol. Bull.* **2018**, *37*, 13.
78. Hou, M.L.; Jiang, S.C.; Jiang, Y.H.; Ling, H.F. S-Pb isotope geochemistry and Rb-Sr isotope chronology of the Penglai gold mineralization in Jiaodong. *J. Petrol.* **2006**, 2525–2533.
79. Shao, J.A.; Mou, B.L.; Zhu, H.Z.; Zhang, C.Q. Deep origin and background of Mesozoic mineralization in the south-central section of the Daxinganling. *J. Petrol.* **2010**, 649–656.
80. Zhu, B.Q. Shell-mantle chemical inhomogeneities and the study of block geochemical boundaries. *Geol. Front.* **1998**, *5*, 72–82.
81. Gao, L.F.; He, Z.H.; Sui, Z.M.; Lu, K.J.; Liu, F.Y. Age, geochemical characteristics of volcanic rocks of the Manketou Ebo formation and their tectonic setting in the Solun area, middle Daxinganling. *Geol. Bull.* **2018**, *37*, 14.
82. Jia, H.M.; Jing, Y.; Wang, Q.H.; Lan, L.X.; Jing, J.H. Genesis of Early Cretaceous granites in the Handaigai area, middle Daxinganling and their geological significance. *World Geol.* **2019**, *38*, 10.
83. Zartman, R.E.; Haines, S.M. The plumbotectonic model for Pb isotopic systematics among major terrestrial reservoirs—A case for bi-directional transport. *Geochim. Cosmochim. Acta* **1988**, *52*, 1327–1339. [[CrossRef](#)]
84. Chu, S.X.; Liu, J.M.; Xu, J.H.; Wei, H.; Chai, H.; Tong, K.G. Zircon U-Pb dating, petrogenesis and tectonic significance of granodiorite diorite from the Sanminggou iron and copper deposit, Heilongjiang. *J. Petrol.* **2012**, *28*, 433–450.
85. Ma, J.J.; Dae-hyuk. Preliminary study of Mesozoic volcanic rocks in Heilongjiang Province. *Heilongjiang Geol.* **1991**, *2*, 16.
86. Lin, W.G. Late mesozoic calc-alkaline volcanism of post-orogenic extension in the northern Da Hinggan Mountains, northeastern China. *J. Volcanol. Geotherm. Res.* **2003**, *121*, 115–135.
87. Meng, Q.R. What drove late Mesozoic extension of the northern China–Mongolia tract? *Tectonophysics* **2003**, *369*, 155–174. [[CrossRef](#)]
88. Zorin, Y.A. Geodynamics of the western part of the Mongolia–Okhotsk collisional belt, trans-Baikal region (Russia) and Mongolia. *Tectonophysics* **1999**, *306*, 33–56. [[CrossRef](#)]
89. Guo, F.; Fan, W.M.; Wang, Y.J.; Lin, G. Late Mesozoic bimodal volcanism in the southern section of the Daxinganling. *J. Petrol.* **2001**, 161–168.
90. Wang, F.; Zhou, X.H.; Zhang, L.C.; Ying, J.F.; Zhang, Y.T.; Wu, F.Y.; Zhu, R.X. Late Mesozoic volcanism in the Great Xing’an Range (NE China): Timing and implications for the dynamic setting of NE Asia. *Earth Planet. Sci. Lett.* **2006**, *251*, 179–198. [[CrossRef](#)]
91. Zhang, L.C.; Zhou, X.H.; Ying, J.F.; Wang, F.; Guo, F.; Wan, B. Geochemistry and Sr-Nd-Pb-Hf isotopes of early Cretaceous basalts from the Great Xing’an Range, NE China: Implications for their origin and mantle source characteristics. *Chem. Geol.* **2008**, *256*, 12–23. [[CrossRef](#)]
92. Xu, M.J.; Xu, W.L.; Wang, F.; Gao, F.H.; Yu, J.J. Chronology and geochemistry of Early Jurassic granitic rocks in central Xiaoxinganling and their tectonic significance. *J. Petrol.* **2013**, *15*.
93. Shao, J.A.; Zhang, L.Q.; Mu, B. Tectono-thermal evolution of middle-south section of the Da Hinggan Mountains. *Sci. China Ser. D: Earth Sci.* **1998**, *41*, 570–579. [[CrossRef](#)]
94. Badarch, G.; Cunningham, W.D.; Windley, B.F. A new terrane subdivision for Mongolia: Implications for the Phanerozoic crustal growth of Central Asia. *J. Asian Earth Sci.* **2002**, *21*, 87–110. [[CrossRef](#)]
95. Chen, C.G.; Zhang, L.C.; Lu, B.C.; Li, Z.L.; Wu, H.Y.; Xiang, P. Age, geochemistry and geological significance of the mineralized porphyry of the Taipingchuan copper-molybdenum mine, Inner Mongolia. *J. Petrol.* **2010**, *26*, 1437–1449.
96. Ying, J.F.; Zhou, R.H.; Zhang, R.C.; Wang, R. Geochronological framework of Mesozoic volcanic rocks in the Great Xing’an Range, NE China, and their geodynamic implications. *J. Asian Earth Sci.* **2010**, *39*, 786–793. [[CrossRef](#)]
97. Sun, D.Y.; Gou, J.; Ren, Y.S.; Fu, C.L.; Wang, L.; Liu, S. U-Pb ages and geochemistry of zircon from volcanic rocks of the Manitou formation, southern Manchuria. *J. Petrol.* **2011**.
98. Li, S.C.; Xu, Z.Y.; Liu, Z.H.; Li, Y.F.; Wang, X.A.; Zhang, C. Age and geochemical characterization of zircon U-Pb from volcanic rocks of the Manitou formation, middle Daxinganling, LA-ICP-MS. *Geol. Bull.* **2013**, *32*, 9.
99. Si, Q.L. Chronology and Geochemistry of Late Mesozoic Volcanic Rocks in the Zalantun Area, Middle Daxinganling. Ph.D. Doctoral Dissertation, Northeastern University, Boston, MA, USA, 2018.
100. Yang, Y.J.; Yang, X.P.; Jiang, B.; Wang, Y.; Pang, X.J. Spatial and temporal distribution of Mesozoic volcanic stratigraphy in Daxing’anling and response to subduction of the Mongolian–Okhotsk and Paleo-Pacific plates. *Geol. Front.* **2022**, *29*, 115–131.
101. Yu, J.J.; Wang, F.; Xu, W.L.; Gao, F.H.; Pei, F.P. Early Jurassic mafic magmatism in the Lesser Xing’an–Zhangguangcai Range, NE China, and its tectonic implications: Constraints from zircon U-Pb chronology and geochemistry. *Lithos* **2012**, *142–143*, 256–266. [[CrossRef](#)]
102. Wu, F.Y.; Sun, D.Y.; Li, H.; Jahn, B.M.; Wilde, S.A. A-type granites in northeastern China: Age and geochemical constraints on their petrogenesis. *Chem. Geol.* **2002**, *187*, 143–173. [[CrossRef](#)]
103. Kravchinsky, V.A.; Cogn, J.P.; Harbert, W.P.; Kuzmin, M.I. Evolution of the Mongol–Okhotsk Ocean as constrained by new palaeomagnetic data from the Mongol–Okhotsk suture zone, Siberia. *Geophys. Res. Astron. Soc.* **2010**, *148*, 34–57. [[CrossRef](#)]

104. Metelkin, D.V.; Gordienko, I.V.; Klimuk, V.S. Paleomagnetism of Upper Jurassic basalts from Transbaikalia: New data on the time of closure of the Mongol-Okhotsk Ocean and Mesozoic intraplate tectonics of Central Asia. *Russ. Geol. Geophys.* **2007**, *48*, 825–834. [[CrossRef](#)]
105. Peng, Y.W.; Chen, Y.J. Location of the tectonic boundary between the Jihei orogenic belt and the Kaiyuan-Shanzhen Town section of the North China Platform. *World Geol.* **2007**, 1–6+74.
106. Zhang, X.Z.; Ma, Y.X.; Chi, X.G.; Zhang, F.X.; Sun, Y.W.; Guo, Y.E. Issues related to the tectonic evolution of the Phanerozoic in Northeast China and East Inner Mongolia. *J. Jilin Univ. Earth Sci. Ed.* **2012**, *42*.
107. Müller, D.; Rock, N.M.S.; Groves, D.I. Geochemical discrimination between shoshonitic and potassic volcanic rocks in different tectonic settings: A pilot study. *Mineral. Petrol.* **1992**, *46*, 259–289. [[CrossRef](#)]

Disclaimer/Publisher’s Note: The statements, opinions and data contained in all publications are solely those of the individual author(s) and contributor(s) and not of MDPI and/or the editor(s). MDPI and/or the editor(s) disclaim responsibility for any injury to people or property resulting from any ideas, methods, instructions or products referred to in the content.